Markov chain Monte Carlo-based Bayesian method for structural model updating and damage detection

Heung-Fai Lam[1], Jia-Hua Yang*[2], and Siu-Kui Au[3]

*Corresponding author: Assistant Professor, Email: javayang@tongji.edu.cn

[1]Department of Architecture and Civil Engineering, City University of Hong Kong, Hong Kong, China

[2]Research Institute of Structural Engineering and Disaster Reduction, College of Civil Engineering, Tongji University, 200092 Shanghai, China

[3]Center for Engineering Dynamics and Institute for Risk and Uncertainty, University of Liverpool, UK

Abstract

This paper proposes a Bayesian method for structural model updating and damage detection using modal data. A recently developed Markov chain Monte Carlo (MCMC) algorithm is adopted to handle the model updating problem. The proposed Bayesian method focuses on calculation of the posterior probability distribution function (PDF) of uncertain model parameters. In addition to the most probable values of the uncertain parameters, the associated uncertainties can be calculated with consideration of the effects of both the modeling error and the measurement noise. An experimental case study was carried out with a shear building model under laboratory conditions to study the identifiability of the model updating problem following the proposed Bayesian method. The results demonstrate the change in the posterior PDF of the uncertain parameters with the amount of measured information. It also demonstrates the ability of the proposed method to handle unidentifiable problems. The proposed Bayesian method is then applied for structural damage detection by calculating the probability distribution of the extent of damage to various structural components. To demonstrate the proposed Bayesian damage detection method, ambient vibration tests were carried out on a two-story steel frame with bolted connections. Joint damage was simulated by loosening some bolts at the target beam-column connection. The model updating results show that the uncertainty associated with the rotational stiffness of the steel joints was very high, rendering the problem almost unidentifiable. Although the problem is almost unidentifiable, the calculated probability distribution of the damage extent can still

locate the damaged joint and estimate the damage extent (i.e., the percentage reduction in rotational stiffness) together with the associated uncertainty.

Keywords: Bayesian modal analysis, Bayesian model updating, Bayesian damage detection, MCMC, uncertainty assessment, ambient vibration test.

1. Introduction

Modal analysis [1-2] and model updating [3-5] have been hot research topics because their integration is useful for detection of structural damage [6-8]. Modal analysis is first carried out to extract the modal parameters (e.g., modal frequencies and mode shapes) from the measured ambient vibration data. Model updating is then conducted to update the stiffness distribution of the computer model so that the model-predicted and identified modal parameters (from the ambient data) are similar. After model updating of the undamaged and possibly damaged structure, possible structural damage can then be identified by comparing the stiffness distributions of the structure at different statuses. Bayesian modal analysis [9-11] has been successfully developed and applied in field tests [12-14]. This paper focuses on the development in Bayesian structural model updating and damage detection.

The efficient performance of model updating and reasonable prediction of the uncertainties in the results is a challenging task. Many deterministic approaches have been developed [15-18], but most of them attempt to conclude a single solution while ignoring other equally important possibilities. Deterministic approaches cannot provide the uncertainties of the results. Probabilistic approaches have been developed to overcome these problems. Beck and Katafygiotis [19] proposed a Bayesian model updating method in which the optimal model was identified by maximizing the posterior PDF of the uncertain structural parameters with optimization techniques. This method works well when the model updating problem is globally or locally identifiable (which may be the case with a large amount of measured data and a low number of uncertain model parameters). The posterior PDF of the uncertain parameters can then be represented by a weighted sum of multivariate Gaussian distributions centered on a finite number of isolated most probable models obtained by minimizing the discrepancy between the measured and model-predicted responses. Note that Katafygiotis and Beck [20] unified the multiple optimums theoretically and developed a computationally efficient numeric algorithm to locate all output-equivalent models in the parameter space of interest. When the information in the data is not sufficient, the model updating problem may become unidentifiable, and the use of Gaussian distributions to approximate the posterior

PDF may not necessarily be accurate. To overcome this difficulty in approximation, a series of well-structured points was generated in the important region in which the value of the posterior PDF exceeded a predefined threshold value [20-21]. One limitation of their method is that the required computational effort grows as the number of uncertain model parameters increases. One advantage, however, is that the points generated in the important region are approximately equally spaced. Once this set of points is available, approximation of the posterior PDF is straightforward and can be very accurate. One promising approach to the solution of unidentifiable model updating problems is to generate samples in the important region(s) of the posterior PDF using MCMC [22]. The posterior PDF is then approximated using the samples. The high-dimension integrals encountered in Bayesian inference can be efficiently computed by Monte Carlo simulation because the computational efficiency does not depend on the dimension of the parameter space. The attractive computational efficiency of MCMC has led to its application for Bayesian model updating and model class selection [23-24], as well as structural health monitoring [25].

In unidentifiable problems with great uncertainties, the posterior PDF is distributed in the neighborhood of an extended and usually highly complex manifold of the parameter space that cannot be calculated in an explicit manner [20-21]. In other words, a continuum of solutions can fit the measured data almost equally well. When more than one optimal model is available, it is essentially impossible to compare the stiffness distributions of undamaged and possibly damaged structures, and damage detection thus becomes difficult or even impossible. Rather than considering a continuum of models in the manifold (i.e., the region with high PDF values), the MCMC method applied in this paper makes it possible to generate a finite number of samples on the manifold for representation (or approximation) of the posterior PDF in unidentifiable cases. It is demonstrated with experimental cases that the method proposed in this paper can handle damage detection even when the corresponding model updating problems are unidentifiable.

This paper proposes a Bayesian method for structural model updating and damage detection using modal data. In the following, the fast Bayesian fast Fourier transform (FFT) modal identification method [9-11] is first reviewed because of its importance in the proposed method. Next, Bayesian model updating based on MCMC is formulated that is applicable for both identifiable and unidentifiable problems. The behavior of the posterior PDF is then experimentally studied using a shear building model when the model updating problem gradually becomes unidentifiable. Furthermore, the Bayesian method for detection of

structural damage is established by calculating the probability distribution of the extent of damage based on the MCMC samples from model updating of undamaged and possibly damaged structures. The method is especially useful for structural damage detection in unidentifiable problems. The proposed Bayesian damage detection method was verified experimentally by detecting joint damage in a 2-story steel frame. From the literature, most Bayesian model updating and damage detection methods are studied by means of computer simulation. One of the contributions of this paper is to demonstrate the applicability of the Bayesian approach with experimental data.

2. Proposed Bayesian method

2.1. Fast Bayesian FFT modal identification

In this paper, modal parameters identified from ambient data are used for damage detection. Reliable modal parameters are crucial for the success of damage detection. The fast Bayesian FFT modal identification method [9-11] makes use of ambient excitations, such as wind excitation and excitations from daily operation of the structure. The method is briefly summarized in this section. The measured acceleration responses at n measured degrees of freedom (DOFs) are defined as $\left\{\hat{\mathbf{u}}_j \in R^n : j = 1,2,\cdots,N\right\}$, where the subscript j represents the sample index and N represents the total number of time steps measured at each DOF. To simplify the formulation, it is represented by $\left\{\hat{\mathbf{u}}_j\right\}$. The FFT of the measured acceleration responses is defined as:

$$\begin{aligned}\mathbf{Fr}_k &= \mathbf{F}_k + \mathbf{i}\mathbf{G}_k \\ &= \sqrt{\frac{2\Delta t}{N}}\sum_{j=1}^{N}\hat{\mathbf{u}}_j \exp\left\{-2\pi\mathbf{i}\left[\frac{(k-1)(j-1)}{N}\right]\right\},\ \text{for } k = 2,3,\ldots,N_q\end{aligned} \tag{1}$$

where the subscript k is the frequency index corresponding to frequency $f_k = (k-1)/(N\Delta t)$; $\mathbf{i}^2 = -1$; $\mathbf{F}_k$ and $\mathbf{G}_k$ are the real and imaginary parts of the FFT, respectively; and Δt is the sampling interval. N_q = int[N/2]+1, where int[.] is the integer operator, which returns the integer part of a number. The modal parameters to be identified are the natural frequency f, the damping ratio ζ, the spectral density of the modal excitation S, and the spectral density of the prediction error σ^2. To facilitate analysis and computation, the negative log likelihood function can be expressed as [9]

$$L\left(f,\zeta,S,\sigma^2\right) = -nN_f \ln 2 + \left(n-1\right)N_f \ln\sigma^2 + \sum_k \ln\left(SD_k + \sigma^2\right) + \sigma^{-2}\left(d - \hat{\lambda}\right) \tag{2}$$

where N_f is the number of FFT values of the selected frequency band, which should be selected so that it includes only one spectral peak in the power spectral density (PSD). D_k is given as follows.

$$D_k = \left(\left(\beta_k^2 - 1\right)^2 + \left(2\zeta\beta_k\right)^2\right)^{-1} \tag{3}$$

where

$$\beta_k = \frac{f}{f_k} \tag{4}$$

$$d = trace\left(\mathbf{A}_0\right) \tag{5}$$

$$\mathbf{A}_0 = \sum_k \mathbf{D}_k \tag{6}$$

$$\mathbf{D}_k = \mathbf{F}_k\mathbf{F}_k^T + \mathbf{G}_k\mathbf{G}_k^T \tag{7}$$

$\hat{\lambda}$ is the maximum eigenvalue of **A**, which is given by

$$\mathbf{A} = \sum_k \left(1 + \sigma^2 / \left(SD_k\right)\right)^{-1}\mathbf{D}_k \tag{8}$$

A summary of the modal identification procedures for a single mode is given as follows.

(1) Measure the acceleration time responses at *n* DOFs of the target structure $\left\{\hat{\mathbf{u}}_j\right\}$.

(2) Select the frequency band in the PSD so that it includes only one spectral peak, and calculate the FFT sequence defined by Eq. (1).

(3) Minimize Eq. (2) to obtain the most probable values of $\{f, \zeta, S, \sigma^2\}$. The minimization is conducted within the selected frequency band. The initial guess of the modal parameters can be found in [9]. The initial guess of the natural frequency f_{in} can be obtained at the spectral peak in the PSD. The initial guess of the damping ratio ζ_{in} is set to 1%. The initial guess of the spectral density of the prediction error σ_{in}^2 is computed according to

$$\sigma_{in}^2 = \frac{d - \lambda_0}{(n-1)N_f} \tag{9}$$

where λ_0 is the maximum eigenvalue of $\mathbf{A}_0$. The initial guess of the spectral density of the modal excitation S_{in} is computed as follows

$$S_{in} = \hat{D}_k \bullet 4\sigma_{in}^2\zeta_{in}^2 \tag{10}$$

where $\hat{D}_k$ represents the maximum eigenvalue of $\mathbf{D}_k$ calculated at the spectral peak.

(4) With the most probable values of $\{f, \zeta, S, \sigma^2\}$ from the minimizing process of step 3, the most probable value of mode shape $\mathbf{\Phi}$ is obtained as the eigenvector of $\mathbf{A}$ in Eq. (8) corresponding to the largest eigenvalue.

2.2. MCMC-based Bayesian model updating

2.2.1. Posterior PDF

The original modal-domain Bayesian formulations of the posterior PDF use the variance of the measured data as the variance of the prediction error [27]. By doing so, the effects of modeling error, which are generally much greater than the effects of measurement noise, are not considered. As a result, the calculated posterior PDF underestimates the uncertainties associated with the model parameters. In this study, the effects of both modeling error and measurement noise are considered by using the fractional error (in a percentage sense). The fractional errors of the natural frequency and mode shape of the a^{th} mode are defined as [28]

$$\varepsilon_{f,a} = \frac{\hat{f}_a - f_a(\mathbf{x})}{\hat{f}_a} \tag{11}$$

$$\varepsilon_{ms,a} = \left(1 - \frac{\left| \hat{\boldsymbol{\psi}}_a^T \boldsymbol{\psi}_a(\mathbf{x}) \right|^2}{\left(\hat{\boldsymbol{\psi}}_a^T \hat{\boldsymbol{\psi}}_a \right) \left(\boldsymbol{\psi}_a^T(\mathbf{x}) \boldsymbol{\psi}_a(\mathbf{x}) \right)} \right)^{\frac{1}{2}} \tag{12}$$

where the subscript a denotes the mode index; $\hat{f}_a$ denotes the identified natural frequency of the a^{th} mode (from the measured ambient data); $f_a(\mathbf{x})$ is the model-predicted frequency whose dependence on uncertain parameter vector $\mathbf{x}$ is emphasized; and $\hat{\boldsymbol{\psi}}_a$ and $\boldsymbol{\psi}_a(\mathbf{x})$ denote the ambient data identified and model-predicted mode shapes, respectively.

The uncertainty in $\varepsilon_{f,a}$ and $\varepsilon_{ms,a}$ is modeled by independent Gaussian distributions with zero mean and the same variance κ^2. The likelihood of the natural frequencies and mode shapes can then be formulated based on the PDFs of the fractional errors. By assuming the uniform PDF as the prior PDF, the posterior PDF of the uncertain parameter vector $\mathbf{x}$ is obtained as follows, according to the Bayesian theorem [28].

$$p(\mathbf{x}|\boldsymbol{D}) = c \exp\left(-\frac{1}{2\kappa^2} J(\mathbf{x}) \right) \tag{13}$$

where $\boldsymbol{D}$ consists of identified natural frequencies and mode shapes (from the measured ambient data); c is a normalizing constant; and the goodness-of-fit function is given as follows

$$J(\mathbf{x}) = \sum_{a=1}^{r} \left[\left(\frac{\hat{f}_a - f_a(\mathbf{x})}{\hat{f}_a} \right)^2 + \left(1 - \left| \hat{\boldsymbol{\psi}}_a^T \boldsymbol{\psi}_a(\mathbf{x}) \right|^2 \right) \right] \tag{14}$$

where r is the number of modes and the identified and predicted modes shapes are normalized so their 2-norms both equal 1.

2.2.2. Markov chain Monte Carlo algorithm

To conduct Bayesian model updating, the posterior PDF must be evaluated. The posterior PDF in practice is usually complicated, and it is not a "well-behaved" PDF. Evaluation of the posterior PDF is therefore a challenging task, especially for unidentifiable problems. The

difficulties were discussed in the Introduction. Our recently developed MCMC algorithm [26-29] is applied in this paper to draw samples according to the posterior PDF. The samples are then used to approximate the posterior PDF. We illustrate that the MCMC algorithm can handle both identifiable and unidentifiable problems. The MCMC algorithm for Bayesian model updating is introduced in the following section.

2.2.2.1. Metropolis-Hastings algorithm

The standard Monte Carlo method, which generates samples directly from the posterior PDF, is not a possible method for model updating. It should be noted that evaluation of the normalizing constant c in Eq. (13) usually requires high-dimension integration, which implies that the constant term in the posterior PDF is not available. This is the common problem for Bayesian methods. Therefore, sampling directly from the posterior PDF is not feasible. Even if the constant is known, the complicated form of the posterior PDF may still prohibit direct sampling. The Metropolis-Hastings (MH) algorithm [30-31], as an MCMC simulation algorithm, does not require the target PDF $p(\mathbf{x})$ to be expressed analytically, and it can be known only up to a multiplicative constant. This is suitable for the solution of Bayesian inference problems. The MH algorithm is given in the following.

Given the current sample $\mathbf{x}^{(i)}$,

(1) Generate the candidate sample $\mathbf{X} \sim q\left(\bullet \middle| \mathbf{x}^{(i)}\right)$.

(2) The next sample is

$$\mathbf{x}^{(i+1)} = \begin{cases} \mathbf{X} & \text{with probability } \rho\left(\mathbf{x}^{(i)}, \mathbf{X}\right), \\ \mathbf{x}^{(i)} & \text{with probability } 1-\rho\left(\mathbf{x}^{(i)}, \mathbf{X}\right), \end{cases}$$

where $\rho(x, y) = \min\left\{\dfrac{p(y)/q(y|x)}{p(x)/q(x|y)}, 1\right\}$

The superscript i denotes the sample index. The proposal density $q\left(\bullet \middle| \mathbf{x}^{(i)}\right)$ is a conditional density that generates samples to approximate the target PDF. $\rho\left(\mathbf{x}^{(i)}, \mathbf{X}\right)$ is called the acceptance probability. The candidate sample has a probability of $\rho\left(\mathbf{x}^{(i)}, \mathbf{X}\right)$ to be accepted;

therefore, the probability for the candidate sample to be rejected is 1 – $\rho\left(\mathbf{x}^{(i)},\mathbf{X}\right)$. If the candidate sample is rejected, the current sample will be treated as the next sample. Note that the candidate sample is always accepted as the next sample if $p(\mathbf{X})/q\left(\mathbf{X}\middle|\mathbf{x}^{(i)}\right) > p\left(\mathbf{x}^{(i)}\right)/q\left(\mathbf{x}^{(i)}\middle|\mathbf{X}\right)$. The MH algorithm will generate samples that constitute a Markov chain whose limit distribution is the target distribution.

Two difficulties prohibit sampling of the posterior PDF with the MH algorithm. First, the posterior PDF in Eq. (13) is not even known up to a scaling constant because κ^2 is undetermined. Second, the important region of the posterior PDF may be much smaller than the parameter space. If one draws samples with the MH algorithm with the posterior PDF treated as the target PDF (assume that the posterior PDF is point-wise known up to a scaling constant), it is very likely that the number of distinct samples will be very small because most candidate samples will be generated in the region of low probability and will be rejected. The sampling process will be very inefficient. In the next section, a sampling scheme is proposed to address these two difficulties and to sample from the complicated posterior PDF.

2.2.2.2. Sampling scheme

The multiple-level sampling scheme [28] like simulated annealing [32-33] is applied in this paper. This sampling scheme is enhanced based on the work in [26]. The multiple-level idea is to divide the entire sampling process into multiple levels and bridge the gap between the initial (prior) PDF and the posterior PDF. A bridge PDF with a large important region is used to generate samples at the beginning of the sampling process. When the sampling process proceeds from one level to the next, the important region of the bridge PDF is reduced in a controlled manner. This process is repeated until the bridge PDF approaches the target posterior PDF. At each level, the MH algorithm is used for sampling, with the bridge PDF as the target PDF at that level. The proposal density of the MH algorithm is the approximation of the bridge PDF constructed by kernel density estimation [34-36] with samples from the previous level. Since the kernel density is constructed by Gaussian PDFs, the applicability of the method depends on the dimension of the problem (i.e., the number of uncertain parameters) [37]. With an appropriate change of the bridge PDF in successive levels, the samples can smoothly travel to the important region of the posterior PDF. The samples generated by the bridge PDF in the final level will be used to approximate the posterior PDF.

The bridge PDF in the g^{th} sampling level is constructed as follows according to Eq. (13)

$$p_g = c_g \exp\left(-\frac{1}{2\kappa_g^2} J(\mathbf{x}) \right) \tag{15}$$

where κ_g^2 reflects the size of the important region of the bridge PDF in the g^{th} sampling level. The relation of κ^2 in two successive sampling levels is given by

$$\kappa_g^2 = \frac{1}{A} \kappa_{g-1}^2 \tag{16}$$

where A (> 1) is an algorithmic parameter that controls the level-to-level change of the bridge PDF. If the value of A is too high, the reduction in the important region within one sampling level is too large. As a result, the MH algorithm will collapse because too many samples will be rejected. If the value of A is too low, many sampling levels will be required and the overall efficiency of the MCMC simulation will be significantly reduced. The rule of choosing A can be found in reference [28]. The value of κ_g^2 is reduced by a factor of $1/A$ at each level. To ensure that the sampling process covers a wide range of parameter space, κ_1^2 is set to 100% at the first sampling level, which is very high in terms of percentage. Following Eq. (16), κ_g^2 is reduced at the following levels, which reflects the decrease of the size of the important region covered by the bridge PDF. Note that an alternative that can efficiently change κ^2 in different levels is the transitional Markov chain Monte Carlo (TMCMC) method [38-39]. The efficiency of TMCMC has been verified on small-scale and full-scale structures.

The sampling process continues until the bridge PDF approaches the target posterior PDF. A stopping criterion is thus needed, which is crucial, especially for damage detection. If the sampling process stops too early, the samples of the uncertain parameters spread out in wide regions and the important region of the posterior PDF cannot not be identified. As a consequence, the samples are not informative, and damage cannot be detected. If the sampling process stops too late, the samples of the uncertain parameters are concentrated in narrow regions and the important region of the posterior PDF is underestimated. A stopping criterion is applied so that the MCMC method can be used for damage detection. The stopping criterion is obtained by determining the best estimate of the measure of prediction error, κ^{*2}, of the bridge PDF in the final sample level

$$\kappa^{*2} = \frac{J^*}{r} \tag{17}$$

where $J^*=J(\mathbf{x}^*)$ is the value of the goodness-of-fit function in Eq. (14) evaluated at the "optimal" point $\mathbf{x}^*$. Note that κ^2 denotes the variance of the fractional error of one mode. The goodness-of-fit function in Eq. (14) is the sum of the squares of the fractional difference between the identified (from the ambient data) and calculated modal parameters for all modes. Eq. (17) is therefore the square of the prediction error averaged over all modes and is a reasonable estimate of the κ^2 value of the target posterior PDF at the final sampling level. Because $J(\mathbf{x})$ is an implicit function of $\mathbf{x}$, the "optimal" value for $\mathbf{x}^*$ is numerically obtained by the active-set algorithm [40] in this study. The value of J^* can then be evaluated numerically using $\mathbf{x}^*$. Once J^* is obtained, the κ^{*2} value of the bridge PDF in the final level can be calculated by Eq. (17). Furthermore, according to Eq. (16), the required number of sampling levels, g_r, can be calculated

$$\kappa_g^2 = \left(\frac{1}{A}\right)^{g-1} \Rightarrow g_r = \text{int}\left(1 - \frac{\ln\left(\kappa^{*2}\right)}{\ln A}\right) \tag{18}$$

where $\kappa_1^2=1$ is used.

2.3. Bayesian structural damage detection

Conventional damage detection methods [17-18] identify an undamaged (reference) model and a damaged model, and the stiffness distributions of the undamaged and damaged structures are compared to detect damage. These methods cannot address the uncertainties of measurement noise and modeling error and are applicable only for identifiable problems. For unidentifiable problems with great uncertainties, an infinite number of models can fit the measured data almost equally well. Keeping only one model and discarding the rest for damage detection will bias the model-predicted results and conclusions on damage. A more rational approach is to consider each of the plausible important models for damage detection. However, when more than one optimal model is available, comparison of the stiffness distributions on a one-to-one basis is impossible. The Bayesian probabilistic method proposed in this paper is applied to address this problem. Instead of pinpointing only one model, multiple models in a model class are included, and their relative plausibility is

considered by their posterior probabilities according to the Bayesian theorem [19, 24-25, 27]. The probability of damage is then calculated based on the class of models for damage detection. In the following section, the probability of damage is derived using the MCMC samples.

Structural damage in this study is defined as the reduction in stiffness (damage extent) of a structural component

$$d_f(i) = \frac{\mathbf{x}_{ud}(i) - \mathbf{x}_d(i)}{\mathbf{x}_{ud}(i)} \tag{19}$$

where **x** denotes the uncertain parameter vector, which consists of the stiffness factors for different components of the target structure. Multiplying the stiffness factors to the nominal stiffness values gives the stiffness of the structure. **x**(*i*) denotes the i^{th} component of the vector **x**. The subscripts *ud* and *d* denote the quantity in the undamaged and potentially damaged states, respectively. Usually, the structure is considered to be damaged if one or more of its components exceeds the predefined threshold value of stiffness reduction. In this study, the probabilities of damage for different components of the structure are calculated. Engineers can then make judgments regarding the structure's damage status. The probability of damage for the i^{th} component of the structural system is formulated according to the total probability theorem as follows.

$$\begin{aligned} P_i^d\left(d_f \middle| \boldsymbol{D}_{ud}, \boldsymbol{D}_d\right) &= P\left(\mathbf{x}_d(i) < \left(1-d_f\right)\mathbf{x}_{ud}(i) \middle| \boldsymbol{D}_{ud}, \boldsymbol{D}_d\right) \\ &= \int_{-\infty}^{+\infty} P\left(\mathbf{x}_d(i) < \left(1-d_f\right)\mathbf{x}_{ud}(i) \middle| \mathbf{x}_{ud}(i), \boldsymbol{D}_d\right) p\left(\mathbf{x}_{ud}(i) \middle| \boldsymbol{D}_{ud}\right) d\mathbf{x}_{ud} \end{aligned} \tag{20}$$

Eq. (20) computes the probability that the stiffness of the i^{th} component of the structure has been reduced by a fraction larger than d_f, given the identification results of the modal parameters of the undamaged and possibly damaged structures, $\boldsymbol{D}_{ud}$ and $\boldsymbol{D}_d$. The integration in Eq. (20) is usually in high dimension. It cannot be evaluated analytically, nor can it be evaluated in a straightforward manner by means of numerical integration. Approximation of Eq. (20) by the MCMC samples is proposed.

$$P_i^d\left(d_f\left|\boldsymbol{D}_{ud},\boldsymbol{D}_d\right.\right)\approx\frac{1}{N_{ss}}\sum_{h=1}^{N_{ss}}P\left(\mathbf{x}_d\left(i\right)<\left(1-d_f\right)\mathbf{x}_{ud}^{(h)}\left(i\right)\middle|\mathbf{x}_{ud}^{(h)}\left(i\right),\boldsymbol{D}_d\right) \tag{21}$$

where the superscript h denotes the sample index. The probability $P\left(\mathbf{x}_d\left(i\right)<\left(1-d_f\right)\mathbf{x}_{ud}^{(h)}\left(i\right)\middle|\mathbf{x}_{ud}^{(h)}\left(i\right),\boldsymbol{D}_d\right)$ can be approximated by a similar manner using the MCMC samples as

$$P\left(\mathbf{x}_d\left(i\right)<\left(1-d_f\right)\mathbf{x}_{ud}^{(h)}\left(i\right)\middle|\mathbf{x}_{ud}^{(h)}\left(i\right),\mathbf{D}_d\right)\approx\frac{1}{N_{ss}}\sum_{z=1}^{N_{ss}}H\left[\left(1-d_f\right)\mathbf{x}_{ud}^{(h)}\left(i\right)-\mathbf{x}_d^{(z)}\left(i\right)\right] \tag{22}$$

where $H(u)$ is a step function. If $u > 0$, $H(u) = 1$. Otherwise, $H(u) = 0$. By substituting Eq. (22) into Eq. (21), the probability of damage can be obtained

$$P_i^d\left(d_f\left|\boldsymbol{D}_{ud},\boldsymbol{D}_d\right.\right)\approx\frac{1}{N_{ss}^2}\sum_{h=1}^{N_{ss}}\sum_{z=1}^{N_{ss}}H\left[\left(1-d_f\right)\mathbf{x}_{ud}^{(h)}\left(i\right)-\mathbf{x}_d^{(z)}\left(i\right)\right] \tag{23}$$

The probabilities of damage for different extents of damage d_f can be calculated with Eq. (23). The cumulative distribution function (CDF) of the damage extent can then be used to identify the damage location and the corresponding damage extent as illustrated in the experimental verification.

2.4. Summary of the proposed Bayesian damage detection method

The main idea is to conduct MCMC-based Bayesian model updating for the undamaged and possibly damaged structures. The probability of damage can then be calculated using the two sets of MCMC samples (see Eq. (23)). The procedure is summarized below.

(1) Set up the initial uniform PDF (which is used as the initial proposal density) of the uncertain model parameters. Decide the value of A, which controls the change in the bridge PDF at each sampling level. Calculate the required number of sampling level g_r with Eq. (18). Set the number of samples N_{ss} in each sampling level. As a rule of thumb, the number of samples should be increased when the complexity of the model class and the number of uncertain model parameters increase.

(2) At the first sampling level (i.e., Level 1): Draw N_{ss} samples with the MH algorithm. Consider the initial uniform PDF as the non-informative PDF and use it as the initial proposal density $q(\bullet|\mathbf{x})$ in the first sampling level. The target PDF of the first sampling level $p(\mathbf{x})$ is constructed by Eq. (15) with the variance $\kappa_g^2 = \kappa_1^2 = 1$ (= 100%).

(3) At the g^{th} sampling level (i.e., Level g): The kernel density of the g^{th} sampling level is k_g, which approximates the bridge PDF in the previous level using samples generated at Level $g-1$. This kernel density k_g is used as the proposal density in the MH algorithm and is given by

$$k_g(\mathbf{x}) = \frac{1}{N_{ss}} \sum_{h=1}^{N_{ss}} \frac{1}{\left(w_o \eta_{g-1}^{(h)}\right)^{n_x}} \mathrm{N}\left(\mathbf{S}_{g-1}^{(h)}, w_o \eta_{g-1}^{(h)} \mathbf{C}_{g-1}\right) \tag{24}$$

where n_x is the dimension of the uncertain parameter vector $\mathbf{x}$. $\mathbf{S}_{g-1}$ is an n_x by N_{ss} matrix, which consists of N_{ss} samples of $\mathbf{x}$. $\mathbf{S}_{g-1}^{(h)}$ denotes the h^{th} sample of $\mathbf{x}$ in Level $g-1$. $\mathrm{N}(\mathbf{c}, \mathbf{d})$ denotes the Gaussian distribution with mean $\mathbf{c}$ and covariance matrix $\mathbf{d}$. $\mathbf{C}_{g-1}$ is the sample covariance matrix computed using samples in $\mathbf{S}_{g-1}$. w_o and $\eta_{g-1}^{(h)}$ are the optimal window bandwidth and the optimal local bandwidth, respectively, whose physical meaning and calculation are given in references [28, 34]. To sample from the kernel density k_g, a sample index $I^{(h)}$ is first drawn from 1 to N_{ss} with the probabilities calculated by

$$W^{(h)} = \frac{\dfrac{1}{\left(w_o \eta_{g-1}^{(h)}\right)^{n_x}}}{\displaystyle\sum_{h=1}^{N_{ss}} \frac{1}{\left(w_o \eta_{g-1}^{(h)}\right)^{n_x}}} \tag{25}$$

By using the sample with the index $I^{(h)}$ and the covariance matrix $\mathbf{C}_{g-1}$, the Gaussian distribution $\mathrm{N}(\bullet,\bullet)$ in Eq. (24) is used to generate a candidate sample at the current level (i.e., the g^{th} sampling level). The MH algorithm with the target PDF constructed by Eq. (15) is used to decide whether this candidate sample is accepted or rejected. This process is continued until all N_{ss} samples are generated and stored in $\mathbf{S}_g$.

(4) Set $g = g + 1$, and repeat steps (3) and (4) until samples of g_r sampling levels are generated.

(5) The posterior PDF and the posterior marginal PDFs of each uncertain parameter are determined by using the samples in the final sampling level g_r. Note that the posterior marginal PDFs can be easily obtained by analytical integration of the kernel density in Eq. (24). The posterior marginal PDF of the i^{th} component in $\mathbf{x}$ can be calculated as

$$k\left(\mathbf{x}(i)\right) = \sum_{h=1}^{N_{ss}} W^{(h)} \mathsf{N}\left(\mathbf{S}_{g_r}^{(h)}(i), \mathbf{C}_{g_r}(i,i)\right) \tag{26}$$

where $\mathbf{S}_{g_r}^{(h)}(i)$ denotes the i^{th} component of the h^{th} sample from the final level g_r; the variance $\mathbf{C}_{g_r}(i,i)$ is the i^{th} diagonal element of the sample covariance matrix calculated by the samples in the final level; and the weightings $W^{(h)}$ can be calculated using Eq. (25) by replacing the level index $g-1$ with g_r.

(6) Conduct steps (1) to (5) (i.e., the model updating process) separately using the identified modal parameters from the undamaged and possibly damaged status to calculate the posterior marginal PDFs of all uncertain parameters in both statuses. The posterior uncertainties of the uncertain parameters are assessed using the posterior marginal PDFs. By following the procedures in section 2.3, the probabilities of damage to different components of the structure are calculated using the MCMC samples in the final sampling level for damage detection.

Some remarks about the computational cost of the proposed method is given here. If the number of uncertain parameters is large, in other words the dimension of the uncertain parameter vector is high, the required number of samples will be large in order to identify the important regions of the posterior PDF. This in turn will increase the computational time as one has to conduct finite element analysis many times.

3. Experimental case study I: Bayesian model updating of a shear building model

3.1. Ambient vibration test and modal analysis of the shear building

A four-story shear building model was constructed in the laboratory (see Figure 1(a)) to illustrate the proposed algorithm for prediction of posterior uncertainties. The shear building

model was made by connecting four rigid steel plates with four steel columns, which were fixed onto the steel base plate by welding. The nominal value of Young's modulus of steel is 200 GPa. Only the vibration along the weak direction is considered, and only translational modes are identified. The dimensions and material properties of the shear building model are summarized in Table 1.

The equipment used in the experiment and the experimental configuration are shown in Figure 1. The vibration was measured with four accelerometers fixed with wax at the middle of the edge of each floor (see Figure 1(a)). Sensors 1 to 4 were installed at floors 1 to 4, respectively, from the bottom to the top. The measured accelerations were transferred through the cables with a special coating, processed with the analog-to-digital device modules (see Figure 1(c)), and recorded by the laptop with LABVIEW. An electric fan (see Figure 1(b)) was used to provide ambient excitation to the shear building to simulate ambient vibration. In the test, 10 minutes of data were measured at a sampling frequency of 2048 Hz. The measured data were then decimated (down-sampled) to 128 Hz for analysis.

The measured acceleration response (unit: $g = 9.81 m/s^2$) from sensor 1 is shown in Figure 2. The vibration of the shear building under wind excitation is apparently statistically stationary. The time domain data were transformed to the frequency domain via FFT (defined in Eq. (1)). The PSDs of the four measured DOFs are plotted together in Figure 3. The four peaks (highlighted with arrows) from the PSDs of the four measured DOFs are consistent, which shows that they are likely to be the four structural modes of the shear building. The corresponding frequencies of the four peaks were used as the initial guess for modal identification using the fast Bayesian FFT method discussed in section 2.1. In total, four modes were identified. The identified natural frequencies are summarized in Table 2, and the identified mode shapes are shown in Figure 4.

3.2. MCMC-based Bayesian model updating

In the structural model for model updating, it is assumed that the masses (see Table 1) are lumped at each floor. The nominal values of the inter-story stiffness k_1 to k_4 of floors 1 to 4 (see Table 1) can be calculated on the basis of the stiffness of the four columns between two floors. By solving the eigenvalue problem, the natural frequencies and mode shapes of the shear building model can be calculated.

Bayesian model updating was carried out by following the MCMC algorithm in section 2.4. The uncertain parameter vector **x** contains four stiffness factors that correspond to the inter-story stiffness of floors 1 to 4. (The numerical values of the inter-story stiffness were equal to the nominal stiffness value multiplied by the corresponding stiffness factor.) To construct the initial uniform PDF of **x**, which is the initial guess about the prior distribution of **x**, the upper and lower bounds of **x** were set to [0;0;0;0] and [5;5;5;5], respectively. The sampling was conducted at multiple levels, and the parameter space was explored with a probabilistic search. The samples of the final level are shown in Figure 5. In the Figure, two uncertain parameters are plotted against each other. The label of the axis, say **x**(1), denotes the first component of **x**, which is the stiffness factor that corresponds to the first floor of the shear building. It can be observed that the samples converge to one region, and the model updating problem is considered to be globally identifiable. The posterior marginal PDFs were calculated using kernel density estimation and are shown in Figure 6 with different markers. The posterior uncertainties of the uncertain parameters can be assessed in Figure 6 by observing the decay of the PDF away from the most probable value (i.e., the peak). It can be concluded that the posterior uncertainties associated with all four inter-story stiffness values are relatively small and that they are similar. Furthermore, all marginal PDFs look like Gaussian distributions. For purposes of comparison, the sample means and sample coefficients of variation (COVs) of the uncertain parameters were calculated with the MCMC samples and their corresponding weightings. The sample means and sample COVs are summarized in Table 3 (refer to the four-mode case). It is clear from the table that the sample COVs of all four uncertain parameters are small because the full set of modal data was used and the posterior uncertainties were small in this case.

The small posterior uncertainties were expected because all modes of the system were considered. In the following, the number of modes used for model updating was reduced step-by-step to study the effects of using different amounts of data on the posterior uncertainties.

3.2.1. Using two modes in model updating

In this part of the study, only the first two identified modes (i.e., modes 1 and 2) were used in the model updating process, and samples were generated using the algorithm in section 2.4. The posterior marginal PDFs are plotted in Figure 7. The posterior marginal PDF of the first uncertain parameter is flat across a wide region. The posterior uncertainties of the other three

uncertain parameters are similar to those with all four modes considered in the model updating process. For this case with two identified modes, the sample means and COVs computed with the MCMC samples are shown in Table 3. When this case is compared to the case with four modes, it is found that the sample COV of the first uncertain parameter increases dramatically and that the sample COVs of the other parameters are similar. The results here show that the posterior uncertainties associated with the identified uncertain parameters are sensitive to the amount of data used in model updating, as expected. The proposed MCMC algorithm provides a systematic and convenient method to assess and compare these uncertainties.

3.2.2. Using one mode in model updating

In this part of the study, only the first identified mode (i.e., mode 1) was used for model updating, and the other conditions were unchanged. The posterior marginal PDFs are shown in Figure 8. The posterior marginal PDFs of the first and fourth uncertain parameters (i.e., the first and fourth inter-story stiffness) are flat, indicating that an infinite number of models can produce the modal parameters that match the identified ones almost as well. The second and third uncertain parameters are still well-identified, and their posterior marginal PDFs are apparently Gaussian. Judging from the posterior marginal PDFs, it can be concluded that the posterior uncertainties of the case with one mode increase dramatically when they are compared with those of the cases with four and two modes. From Table 3, the sample COVs of the first and fourth uncertain parameters in the one-mode case are much larger than those in the cases with four and two modes.

It can be concluded that a given uncertain parameter could be sensitive to some modes but not to the others. If the sensitive modes are not considered in the model updating process, the uncertainty associated with that uncertain parameter could increase significantly. It can be further concluded that when only the first two modes are considered, the model updating problem becomes unidentifiable and one of the uncertain parameters is unidentifiable. When only one mode is considered, the unidentifiable problem becomes serious, and two of the four uncertain parameters are unidentifiable.

4. Experimental case study II: structural joint damage detection of a steel frame

4.1. Ambient vibration test and modal analysis of the steel frame

A two-story steel frame (see Figure 9) was used to conduct damage detection to verify the proposed method. The width of this steel frame was about 2.00 m, and its height was about 2.50 m. There were six connections: (1) the top-left beam-column joint, (2) the top-right beam-column joint, (3) the middle-left beam-column joint, (4) the middle-right beam-column joint, (5) the bottom-left column-base joint, and (6) the bottom-right column-base joint. The numbering of the joints is given in Figure 9(a), where **x** denotes the vector of the uncertain parameters and **x**(1) to **x**(6) are stiffness coefficients of six equivalent rotational springs to model the flexibility in the joints. Note that the joints were bolted connections and that neither the beam-column joints nor the column-base joints were completely rigid (see Figure 9(c, d)). Rotational springs were used at the six joints in the computer model of this steel frame to capture the system's semirigid behavior.

The equipment used was the same as that in shear building case study I (Section 3). An electric fan (see Figure 9(b)) was used to simulate the wind excitation. Only 11 accelerometers were available for this vibration test. To obtain the mode shapes of the steel frame, four setups of measurements were designed and implemented. Eleven sensors were used for each setup. The configurations of the sensors in the four setups and the instrumented locations (represented by circular marks) are presented in Figure 10. In the figure, the numbers denote the numbering of the sensors. The sensors installed on the columns measure only the horizontal vibration, and the sensors installed on the beams measure only the vertical vibration. It can be seen that the four setups in Figure 10(a), (b), (c), and (d) are configured to the measurements of the left column, the upper beam, the lower beam, and the right column, respectively. The repeated sensors among the four setups, such as sensors 1, 9, 10, and 11, were reference sensors that were used to assemble the partial mode shapes identified from different setups.

The experiment for the undamaged steel frame was conducted first. The PSDs corresponding to the first setup are shown in Figure 11. The PSDs of all DOFs in the first setup are plotted in the same figure. Seven structural modes were identified, and their spectral peaks are highlighted by arrows in Figure 11. The identified natural frequencies and mode shapes of the steel frame are presented in Table 4 and Figure 12. Except for the first and second modes, in which the vibration of the beams is small and the column vibration dominates, it can be seen that beam vibration couples with column vibration for the rest of the modes. The "sine curve" shape in the beams and columns shows that these modes are typical bending modes. These seven modes were used in the model updating of the steel frame.

4.2. Bayesian model updating for the undamaged steel frame using MCMC

The computer model of the steel frame was established using the finite element method. Rotational springs were used to model the semirigid behavior of the steel joints. The locations of the rotational springs are illustrated by six uncertain rotational stiffness parameters **x**(1) to **x**(6) in Figure 9(a). The rotational stiffness of the different joints need not be the same, and separate parameterization is thus necessary. The nominal values of rotational stiffness at the six locations are given in Table 5. For this type of structure, damage is common at the structural joints. Therefore, the purpose of this study focused on the detection of damage at the six joints of the steel frame. Six uncertain parameters **x**(1) to **x**(6) (see Figure 9(a)) were used to scale the nominal rotational stiffness of the joints. MCMC was then conducted to update the uncertain parameters for the undamaged steel frame to obtain a reference system. The initial uniform distribution of the uncertain parameters was constructed by assuming that they were uniformly distributed in a region whose lower and upper bounds were defined by [0;0;0;0;0;0] and [10;10;10;10;10;10], respectively. The posterior marginal PDFs are shown in Figure 13. The distributions of the rotational stiffness at locations 1 and 2 (i.e., **x**(1) and **x**(2)) cover smaller regions than those of other distributions, implying that the uncertainties associated with the first two uncertain parameters are smaller than those associated with others based on the set of measured data. Because the parts of the PDFs for negative values of **x** were truncated, these PDFs do not follow Gaussian distributions. The posterior marginal PDFs of rotational stiffness at all joints show that the model updating problem is almost unidentifiable [41] because their uncertainties are very high, especially for **x**(5) and **x**(6). The projection of the posterior samples on the **x**(5)-**x**(6) plane is presented in Figure 14. The broad distribution of the samples on this plane can be observed. It leads to the broad single peak shown by each marginal PDF for **x**(5) and **x**(6).

Many methods use a single “optimal” model for damage detection or response prediction. In this almost unidentifiable case, it is not reasonable to use a single “optimal” model for damage detection. It is clear from the posterior marginal PDF in Figure 13 that the important region of **x** occupies a wide range of the parameter space and that the “optimal” model is just one of many models that possess relatively high plausibility. The justification for keeping only the “optimal” model and discarding the rest is weak. A reasonable method of damage detection in this case is to consider all models in the important region of the parameter space, with the posterior PDF used to measure these models’ relative plausibility. The following

damage detection case shows that the proposed method can handle unidentifiable problems with acceptable computational effort.

4.3. Bayesian damage detection of the steel frame

Structural damage was physically simulated at the top right joint (i.e., **x**(2)). In this damage case, the bolts at the top angle were loosened to reduce the rotational stiffness and the bottom angle was untouched. The damage scenario is shown in Figure 15. The experiment was carried out in a manner similar to that of the undamaged case. MCMC was conducted to generate samples to obtain the posterior PDF of the rotational stiffness values at the six joints. The posterior marginal PDFs are plotted in Figure 16. It can be easily observed that the spread of the posterior marginal PDFs of all rotational stiffness values is very large (covering a wide range of parameter values) except for **x**(2). The model updating problem is almost unidentifiable.

After model updating is conducted for the undamaged and damaged steel frame, damage detection can be carried out by calculating the probabilities of damage for the six rotational stiffness values. Note that the model updating problems that correspond to both the undamaged and damaged situations are almost unidentifiable. This significantly increases the difficulty of structural damage detection. Because both the undamaged and damaged cases have an infinite number of models with nearly equal posterior plausibility, it is challenging to make a direct comparison of the stiffness distributions from the undamaged and damaged cases. Eq. (23) was used to calculate the damage probabilities of the uncertain parameters for different damage extents d_f. The calculated probabilities of damage are summarized in Figure 17, which is the plot of cumulative probability function (CDF). For a particular damage extent d_f in this figure, the probability that the damage extent of the target structural component is larger than d_f can be obtained. This figure enables the health status of the target structure to be assessed. First, it is observed that the curve for **x**(2) (i.e., the rotational stiffness at the top right joint of the frame) is the most outstanding curve and that it lies in the upper part of the figure, which indicates a high probability of damage at the top right joint (i.e., **x**(2)). This is consistent with the actual damage. Second, to confirm the damage, the median [42], is used to quantify the damage in an average sense. A bold horizontal line at a probability of 0.5 is drawn in Figure 17, and the intersections between the bold horizontal line and the six curves indicate the median losses of stiffness at the six joints. The median stiffness loss at the top right joint (**x**(2)) is 0.634 (i.e., 63.4% reduction in stiffness), which is

a great loss. The meaning is that the probability that the stiffness loss of $\mathbf{x}(2)$ is larger than 0.634 is 0.5. It is worth noting that by loosening half of the joint (e.g., loosening only the top angle but not the bottom one), the loss in joint stiffness is approximately 50%. This value is near the predicted median stiffness loss of 63.4% by the proposed method. It demonstrates that the proposed Bayesian method can be used to identify the damaged location and to reasonably predict the extent of damage. Based on the damage detection result, the proposed method detected the damage at the top right joint, which was consistent with the actual damage. Moreover, the median losses of stiffness in the other five joints were low enough that these five joints were considered to be undamaged.

4. Conclusions

In this paper, a Bayesian method for structural model updating and damage detection based on MCMC was developed. One important contribution is that the experimental observations from the two case studies offer insights into the Bayesian framework, which is usually studied numerically in the literature. The main idea of the proposed method is to conduct Bayesian model updating to identify the posterior PDF of the stiffness distributions of undamaged and possibly damaged structures. The damage in the target structure is then detected by calculating the probability of damage at various structural components. In the proposed method, Bayesian model updating is carried out with MCMC. The posterior PDF is sampled to locate its important region. However, direct sampling is inefficient because the important region of the posterior PDF is small compared to the parameter space, and the chance of the sampling process hitting it is thus very small. To overcome this difficulty, a multiple-level sampling scheme was adopted to explore the parameter space. Bridge PDFs were constructed in multiple levels in such a way that their important regions decreased gradually and moved toward the important region of the posterior PDF. The difference between the bridge PDFs at two successive levels was sufficiently small for the samples to move smoothly toward that region. The MH algorithm was repeatedly applied at each level, and the bridge PDF was used as the target PDF. The kernel density, which approximates the bridge PDF, is used as the proposal density. The posterior marginal PDFs of the uncertain model parameters can be easily obtained on the basis of the samples from the final sampling level without high-dimensional numerical integration, and the posterior uncertainties can be assessed by the posterior marginal PDFs. Damage detection is based on the CDF of the damage extent, which is computed with the MCMC samples. This CDF allows the

assessment of damage location and extent together with the associated uncertainties. Damage detection for unidentifiable problems can be tackled using this CDF of the damage extent.

It should be noted that the rigorous approach is to include κ as an uncertain parameter and conduct sampling for κ. However, if sampling is also conducted for κ, the size of the important region of the bridge PDF will be difficult to control. It is possible that the sampling is conducted in a wide region of the parameter space and the convergence speed will be very slow, and the computational cost will be large for structures in practice (like the case in this paper). To maintain an affordable computational cost, κ is controlled such that it is decreased gradually level by level. In addition, κ is determined based on the measured data using Eq. (17) and the resulting value is considered to be the approximated most probable value. The posterior PDF is thus used without being conditional on κ. The rigorous approach will be the future work.

It is also worth mentioning that the proposed method can be also considered to be an optimization algorithm. However, there are differences between the proposed method and traditional optimization algorithms. The proposed method systematically explores the parameter space, which has the promise of including all equally-important solutions. Most of traditional optimization algorithms try to pinpoint one solution and the locally-trapped solution may bias the performance of the identified model in a model updating problem. Moreover, when used as an optimization algorithm, the proposed algorithm can provide most probable values together with the corresponding uncertainties, whereas most traditional optimization algorithms give only optimal solutions.

Experimental case studies were used to verify the proposed Bayesian method. In the first experimental verification, a shear building model was adopted. The ambient modal analysis was carried out to obtain the modal parameters, and different amounts of modal data were applied for model updating of this shear building. The results indicate that the proposed Bayesian method can predict the posterior uncertainties with reasonable accuracy. When all of the measured data are included, the problem is globally identifiable and the posterior uncertainties are small. When the amount of modal data is reduced, the uncertainties increase, as indicated by the flat posterior marginal PDF in a wide range. When the amount of modal data is further trimmed, some uncertain parameters become almost unidentifiable.

Structural damage detection with the proposed method was investigated in a two-story steel frame, and the corresponding model updating problem is almost unidentifiable. There are

infinitely many solutions that provide a very similar fit to the measured data, so the stiffness reduction cannot be directly computed, which makes damage detection a difficult task. The experimental case study demonstrates that the location of damage can be identified and that the damage extent can also be reasonably predicted by assessing the CDF of damage.

Acknowledgement

The work described in this paper was supported by the Research Grants Council of the Hong Kong Special Administrative Region, China (Project No. 9041889 (CityU 115413)).

References

1. Brownjohn JMW. Ambient vibration studies for system identification of tall buildings. *Earthquake Engineering & Structural Dynamics* 2003; **32**(1): 71-95.

2. Brownjohn JMW, Magalhaes F, Caetano E, and Cunha A. Ambient vibration re-testing and operational modal analysis of the Humber Bridge. *Engineering Structures* 2010; **32**(8): 2003-2018.

3. Yuen KV, Beck JL, and Katafygiotis LS. Efficient model updating and health monitoring methodology using incomplete modal data without mode matching. *Structural Control and Health Monitoring* 2006; **13**(1): 91-107.

4. Brownjohn JM and Xia PQ. Dynamic assessment of curved cable-stayed bridge by model updating. *Journal of Structural Engineering* 2000; **126**(2): 252-60.

5. Lam HF, Peng HY, and Au SK. Development of a practical algorithm for Bayesian model updating of a coupled slab system utilizing field test data. *Engineering Structures* 2014; **79**: 182-194.

6. Yuen KV, Beck JL, and Katafygiotis LS. Unified probabilistic approach for model updating and damage detection. *Journal of Applied Mechanics* 2006; **73**(4): 555-64.

7. Sohn H and Law KH. A Bayesian probabilistic approach for structure damage detection. *Earthquake Engineering & Structural Dynamics* 1997; **26**: 1259-1281.

8. Lam HF and Yang JH. Bayesian structural damage detection of steel towers using measured modal parameters. *Earthquakes and Structures* 2015; **8**(4): 935-56.

9. Au SK. Fast Bayesian FFT method for ambient modal identification with separated modes. *Journal of Engineering Mechanics* 2011; **137**(3): 214-226.

10. Au SK. Fast Bayesian ambient modal identification in the frequency domain, Part I: Posterior most probable value. *Mechanical Systems and Signal Processing* 2012; **26**: 60-75.

11. Au SK. Fast Bayesian ambient modal identification in the frequency domain, Part II: Posterior uncertainty. *Mechanical Systems and Signal Processing* 2012; **26**: 76-90.

12. Ni YC and Zhang FL. Bayesian operational modal analysis of a pedestrian bridge using a field test with multiple setups. *International Journal of Structural Stability and Dynamics* 2015: 1550052.

13. Zhang FL, Ni YQ, and Ni YC. Mode identifiability of a cable-stayed bridge based on a Bayesian method. *Smart Structures and Systems* 2016; **17**(3): 471-89.

14. Zhang FL, Ni YQ, Ni YC, and Wang YW. Operational modal analysis of Canton Tower by a fast frequency domain Bayesian method. S*mart Structures and Systems* 2016; **17**(2): 209-230.

15. Hua XG, Ni YQ, and Ko JM. Adaptive regularization parameter optimization in output-error-based finite element model updating. *Mechanical Systems and Signal Processing* 2009; **23**(3): 563-79.

16. Ni YQ, Xia Y, Lin W, Chen WH, and Ko JM. SHM benchmark for high-rise structures: a reduced-order finite element model and field measurement data. *Smart Structures and Systems* 2012; **10**(4-5): 411-26.

17. Hao H and Xia Y. Vibration-based damage detection of structures by genetic algorithm. *Journal of Computing in Civil Engineering* 2002; **16**(3): 222-9.

18. Yin T, Lam HF, Chow HM, and Zhu HP. Dynamic reduction-based structural damage detection of transmission tower utilizing ambient vibration data. *Engineering Structures* 2009; **31**: 2009-2019.

19. Beck JL and Katafygiotis LS. Updating models and their uncertainties. I: Bayesian statistical framework. *Journal of Engineering Mechanics* 1998; **124**(4): 455-461.

20. Katafygiotis LS and Beck JL. Updating models and their uncertainties. II: Model identifiability. *Journal of Engineering Mechanics* 1998; **124**(4): 463-7.

21. Papadimitriou C, Beck JL, and Katafygiotis LS. Updating robust reliability using structural test data. *Probabilistic Engineering Mechanics* 2001; **16**(2): 103-13.

22. Robert CP and Casella G. Monte Carlo statistical methods. New York: Springer, 2004.

23. Cheung SH and Beck JL. Calculation of posterior probabilities for Bayesian model class assessment and averaging from posterior samples based on dynamic system data. *Computer-Aided Civil and Infrastructure Engineering* 2010; **25**(5): 304-321.

24. Muto M and Beck JL. Bayesian updating and model class selection for hysteretic structural models using stochastic simulation. *Journal of Vibration and Control* 2008; **14**(1-2): 7-34.

25. Yuen KV, Beck JL, and Au SK. Structural damage detection and assessment by adaptive Markov chain Monte Carlo simulation. *Structural Control and Health Monitoring* 2004; **11**(4): 327-347.

26. Beck JL and Au SK. Bayesian updating of structural models and reliability using Markov Chain Monte Carlo simulation. *Journal of Engineering Mechanics* 2002; **128**(4): 380-391.

27. Beck JL, Au SK, and Vanik MW. Monitoring structural health using a probabilistic measure, *Computer-Aided Civil and Infrastructure Engineering* 2001; **16**: 1-11.

28. Lam HF, Yang JH, and Au SK. Bayesian model updating of a coupled-slab system using field test data utilizing an enhanced Markov chain Monte Carlo simulation algorithm. *Engineering Structures* 2015; **102**: 144-155.

29. Yang JH, Lam HF, and Hu J. Ambient vibration test, modal identification and structural model updating following Bayesian framework. *International Journal of Structural Stability and Dynamics* 2015; 1540024.

30. Metropolis N, Rosenbluth A, Rosenbluth MN, Teller AH, and Teller E. Equations of state calculations by fast computing machines. *Journal of Chemical Physics* 1953; **21**(6): 1087-1091.

31. Hastings WK. Monte Carlo sampling methods using Markov chains and their applications. *Biometrika* 1970; **57**(1): 97-109.

32. Geyer CJ and Thompson EA. Annealing Markov chain Monte Carlo with applications to ancestral inference. *Journal of the American Statistical Association* 1995; **90**(431): 909-920.

33. Neal RM. Annealed importance sampling. *Statistics and Computing* 2001; **11**(2): 125-139.

34. Au SK and Beck JL. A new adaptive importance sampling scheme. *Structural Safety* 1999; **21**: 135-158.

35. Ang GL, Ang AHS, and Tang WH. Optimal importance sampling density estimator. *Journal of Engineering Mechanics* 1992; **118**(6): 1146-1163.

36. Silverman BW. Density estimation for statistics and data analysis (Vol. 26). Boca Raton, FL: CRC Press, 1986.

37. Au SK and Beck JL. Important sampling in high dimensions. *Structural Safety* 2003; **25**(2): 139-163.

38. Ching JY and Chen YC. Transitional Markov chain Monte Carlo method for Bayesian model updating, model class selection, and model averaging. *Journal of Engineering Mechanics* 2007; **133**: 816–832.

39. Angelikopoulos P, Papadimitriou C and Koumoutsakos P. X-TMCMC: Adaptive kriging for Bayesian inverse modeling. *Computer Methods in Applied Mechanics and Engineering* 2015; **289**: 409-428.

40. Nocedal J and Wright SJ. Numerical optimization (2nd ed.). Berlin: Springer-Verlag, 2006.

41. Katafygiotis LS and Lam HF. Tangential-projection algorithm for manifold representation in unidentifiable model updating problems. *Earthquake Engineering and Structural Dynamics* 2002; **31**(4): 791-812.

42. DeGroot MH and Schervish MJ. Probability and statistics (4th ed.). London: Pearson Education, 2011.

(a) Shear building model.

(b) Electric fan.

(c) NI-9234 A/D converter

Figure 1. Experimental setup.

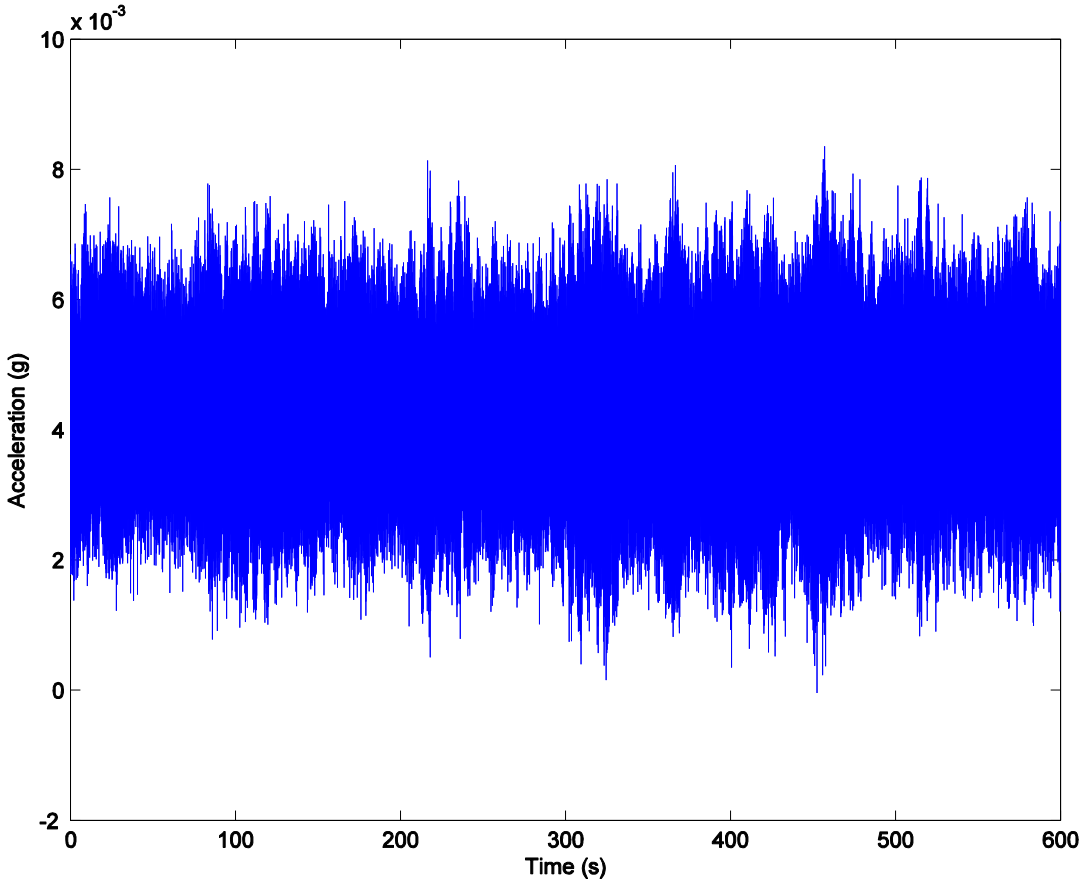

Figure 2. Acceleration response of sensor 1 of shear building.

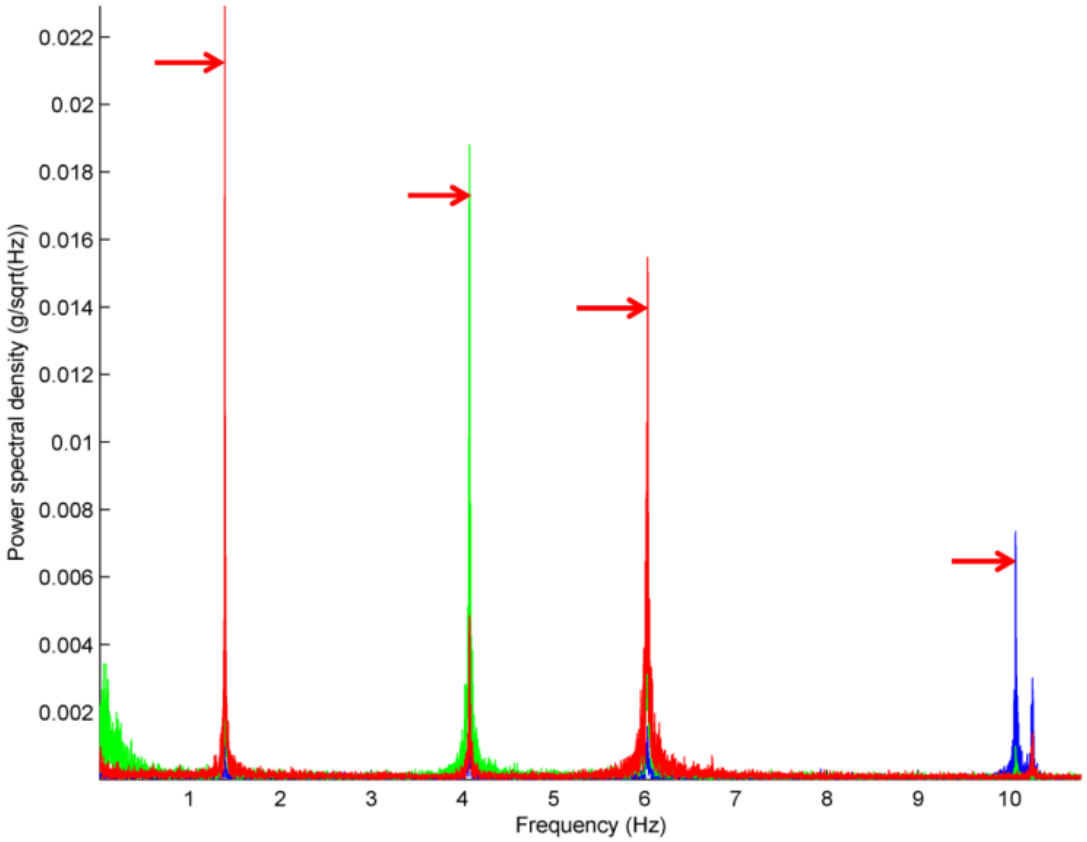

Figure 3. PSDs of shear building.

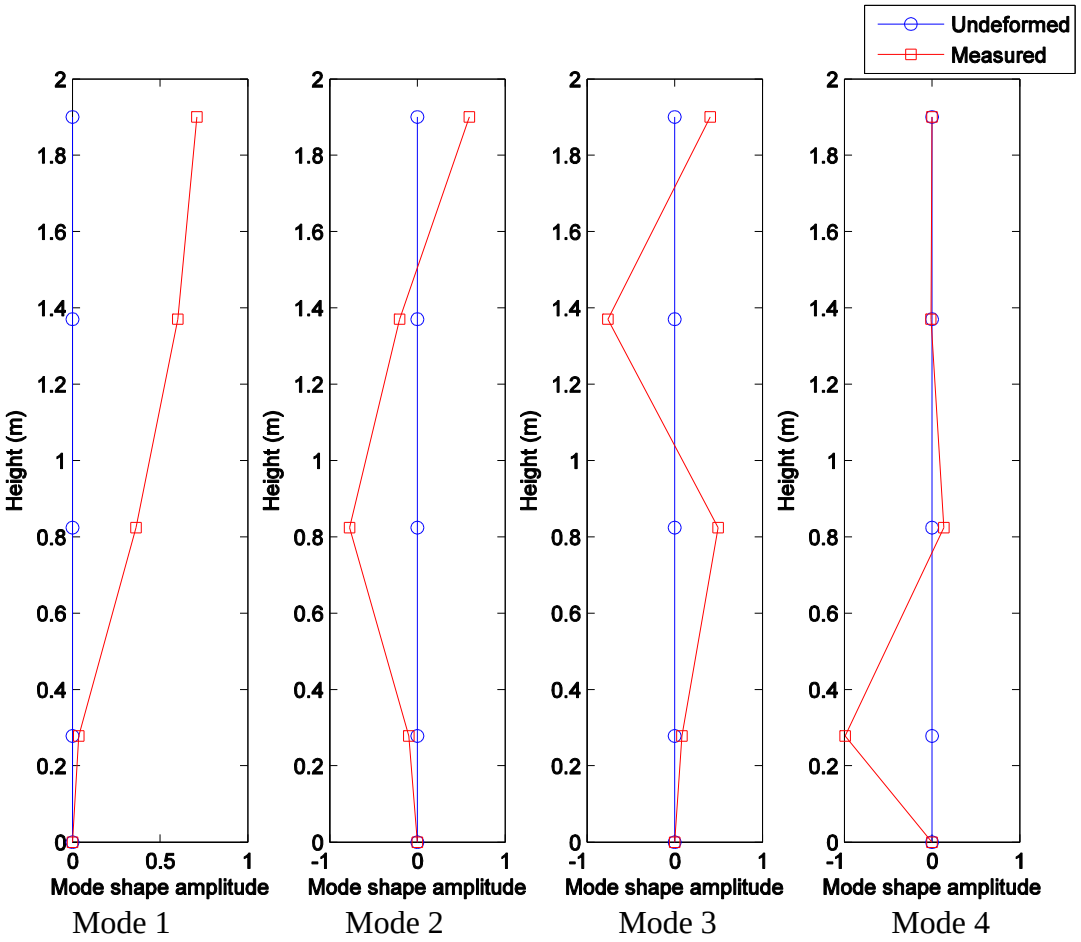

Figure 4. Identified mode shapes of shear building.

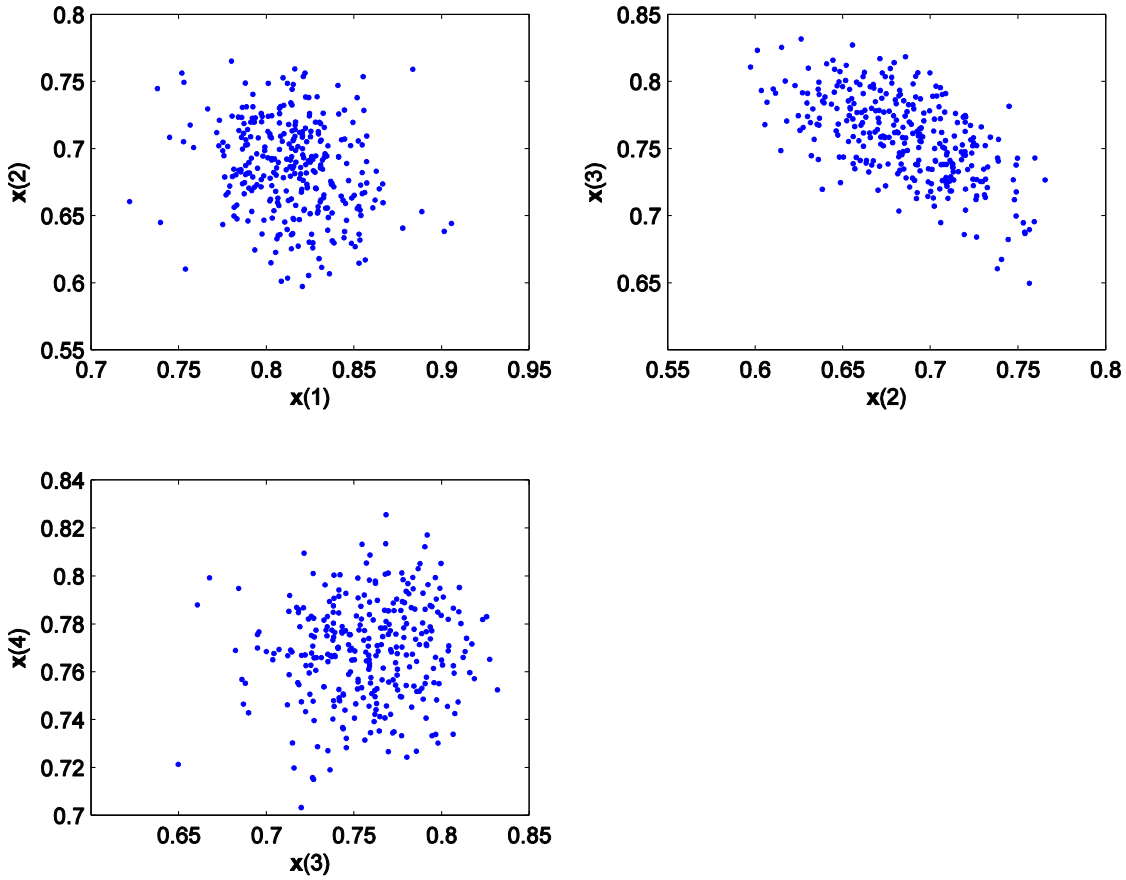

Figure 5. Samples of final level for shear building using four modes.

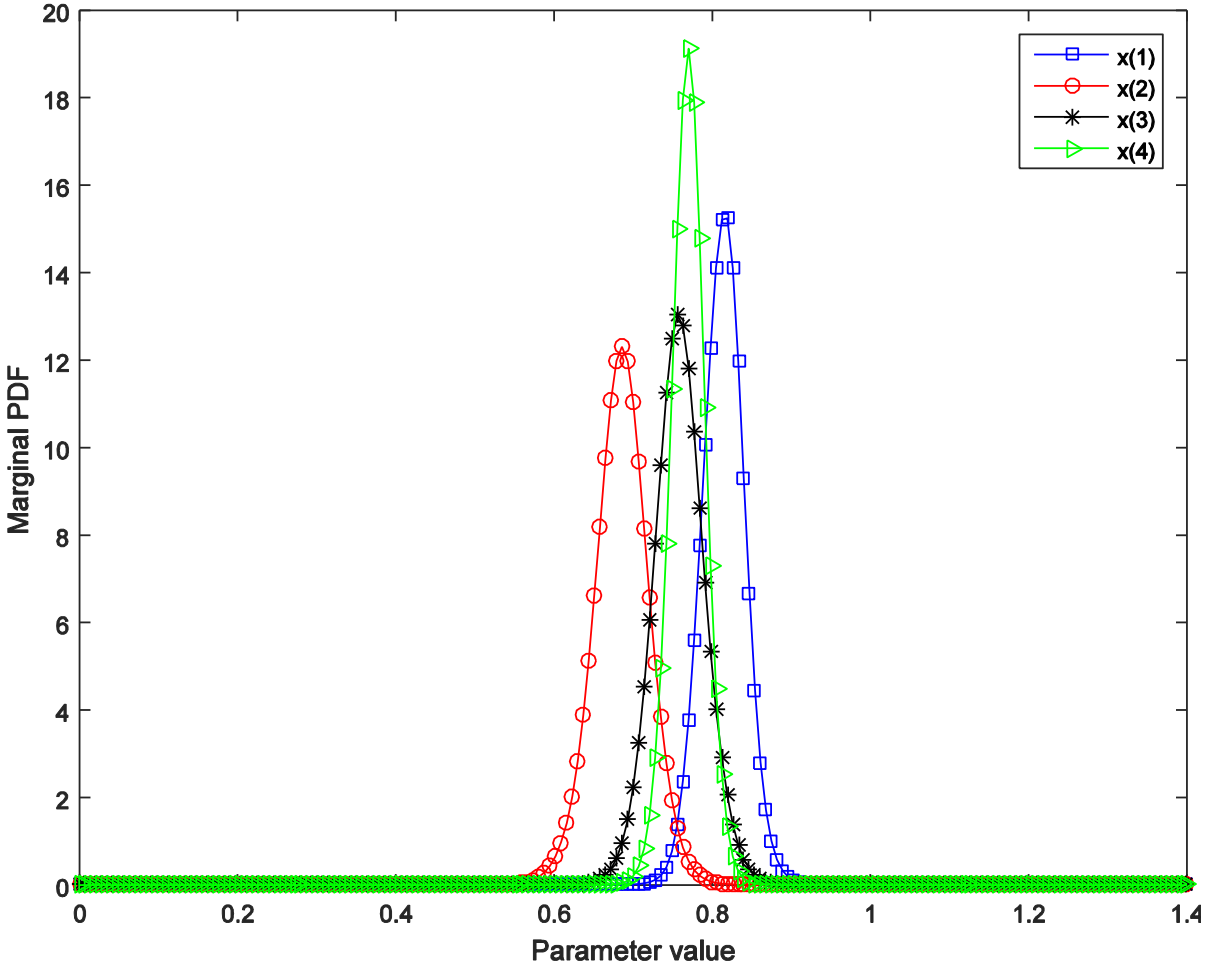

Figure 6. Posterior marginal PDFs for shear building using four modes.

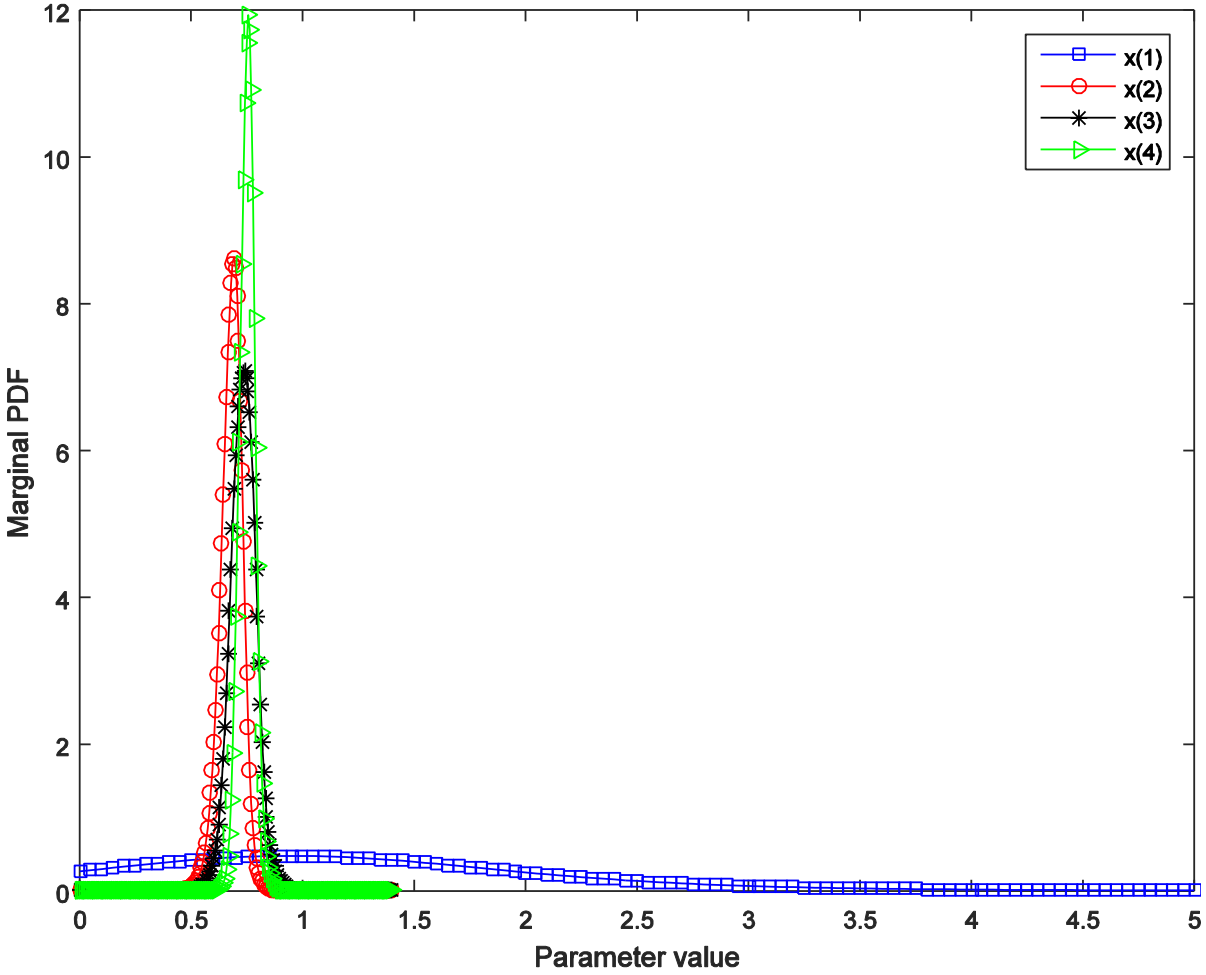

Figure 7. Posterior marginal PDFs for shear building using two modes.

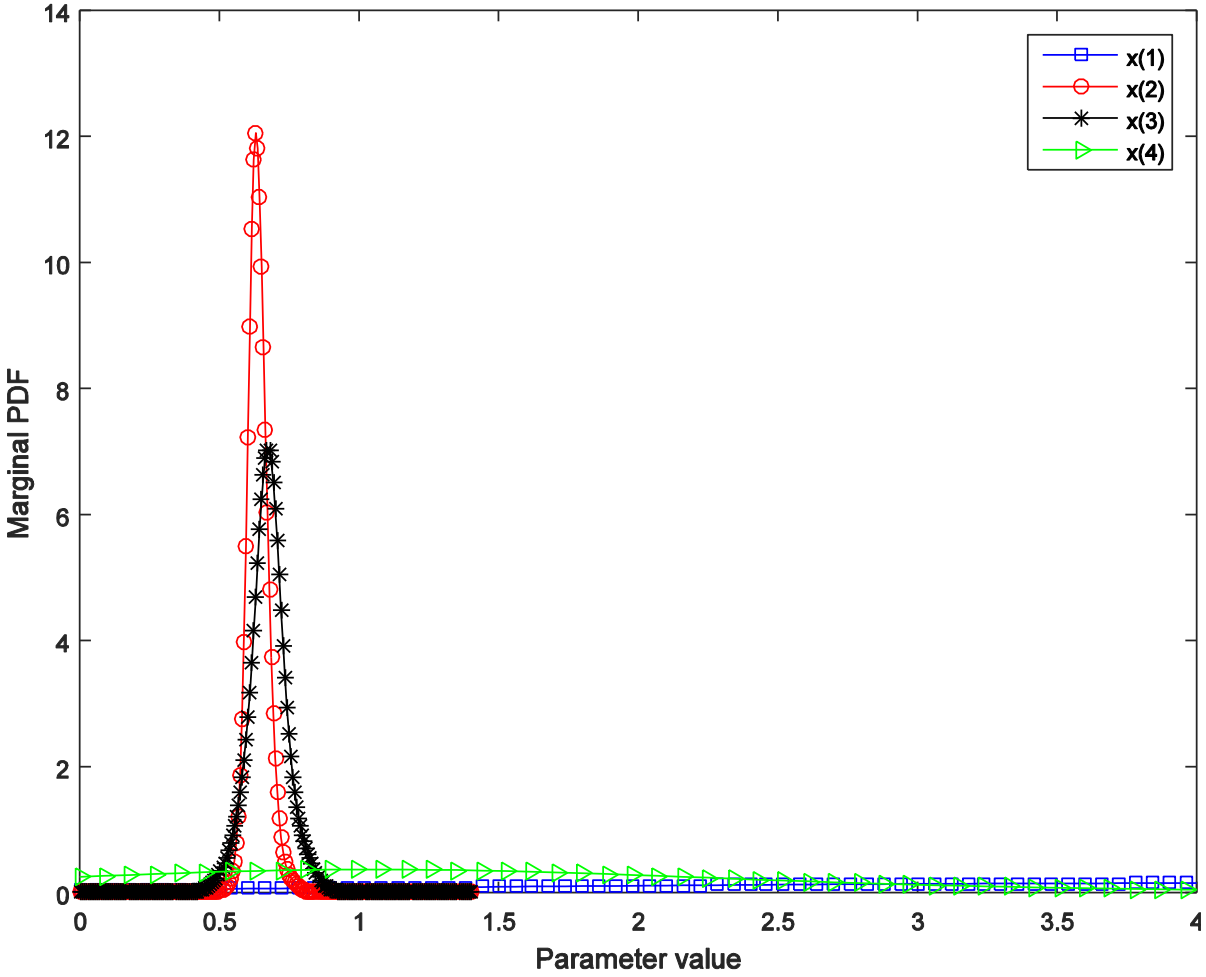

Figure 8. Posterior marginal PDFs for shear building using one mode.

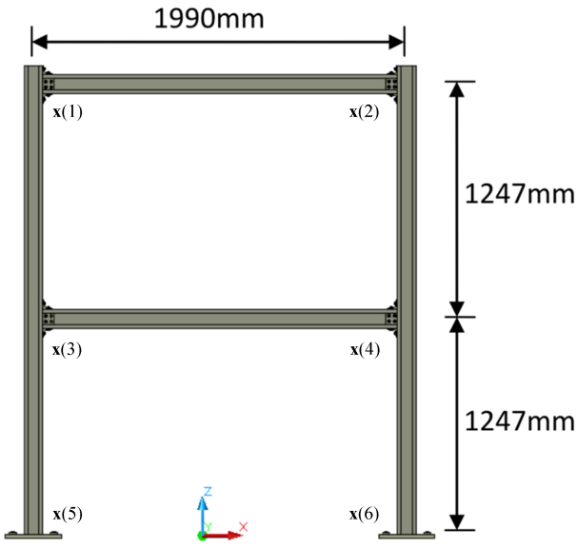

(a) Dimensions of steel frame.

(b) Steel frame under wind load.

(c) Beam-column joint.

(d) Column-base joint.

Figure 9. Two-story steel frame.

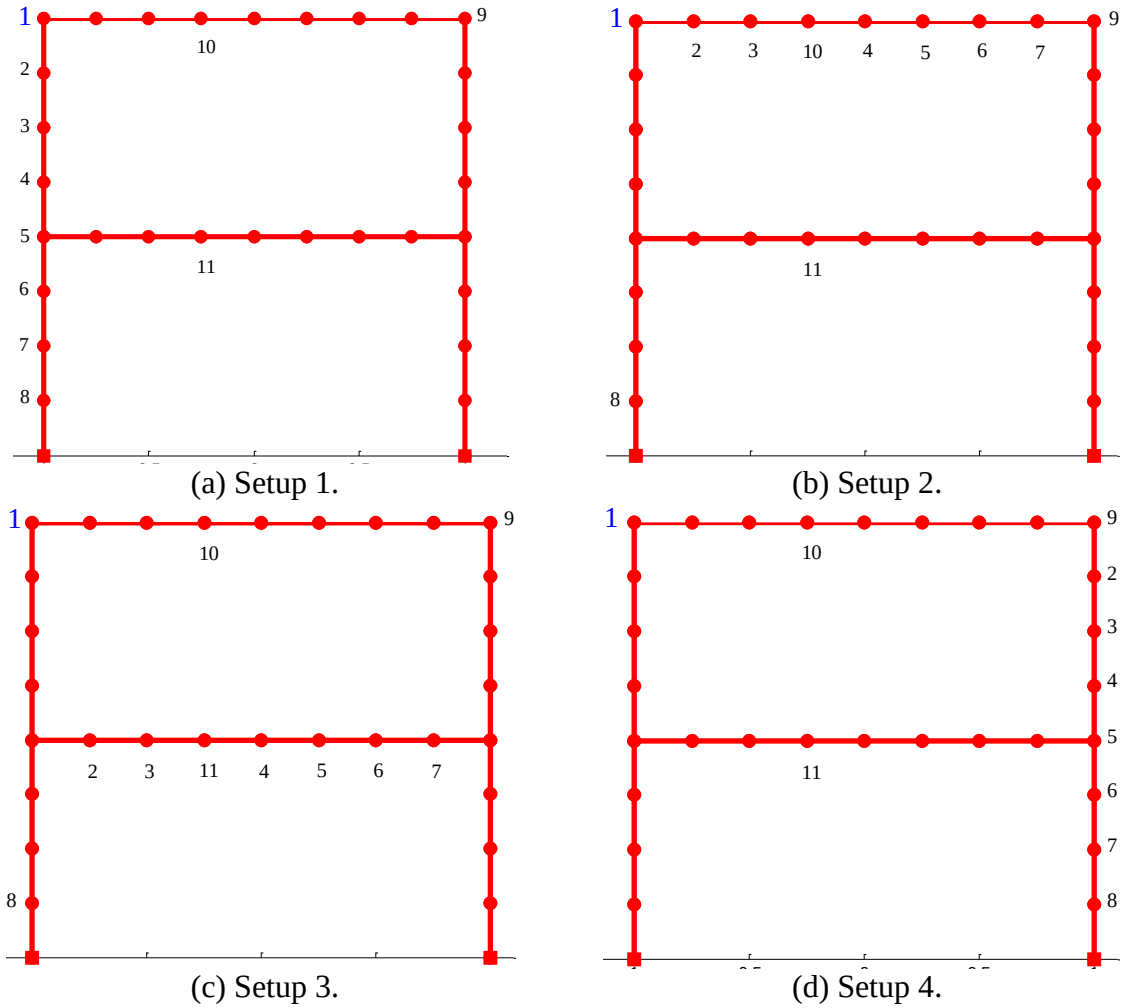

Figure 10. Configuration of sensors.

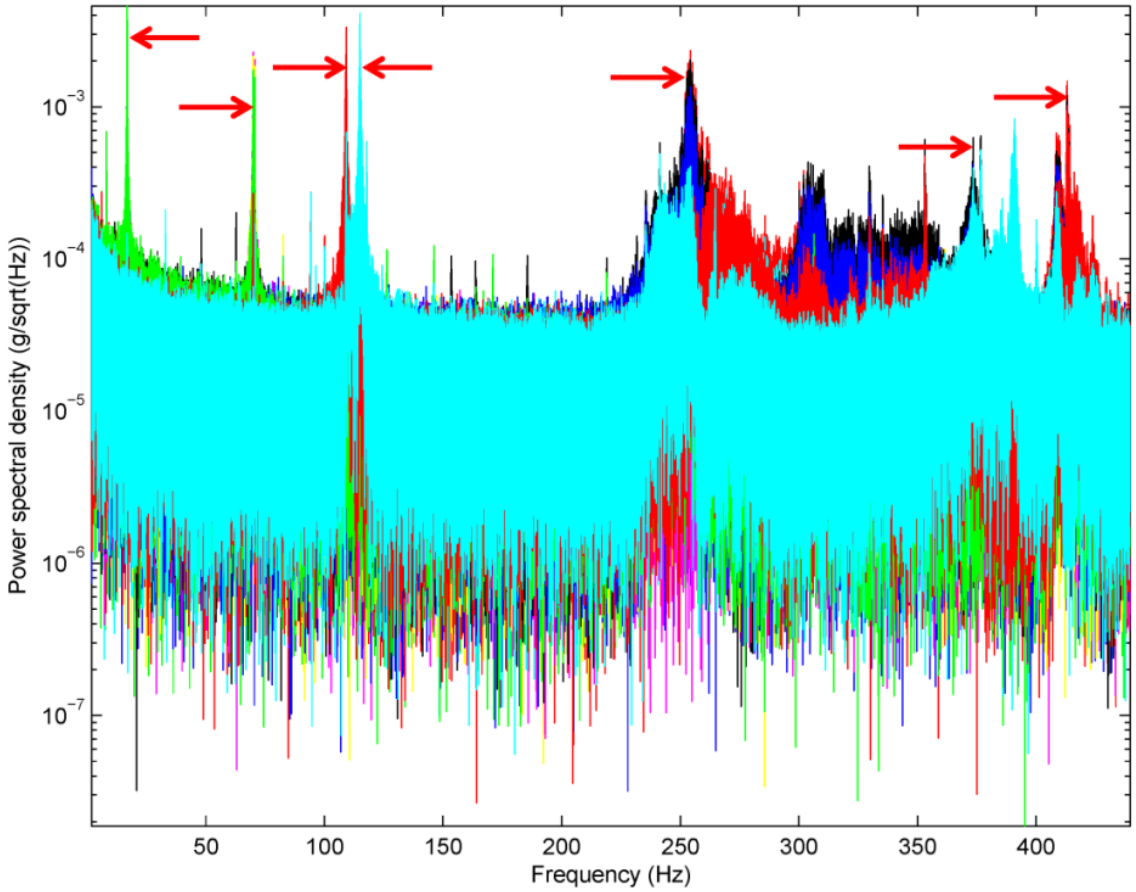

Figure 11. PSDs of steel frame.

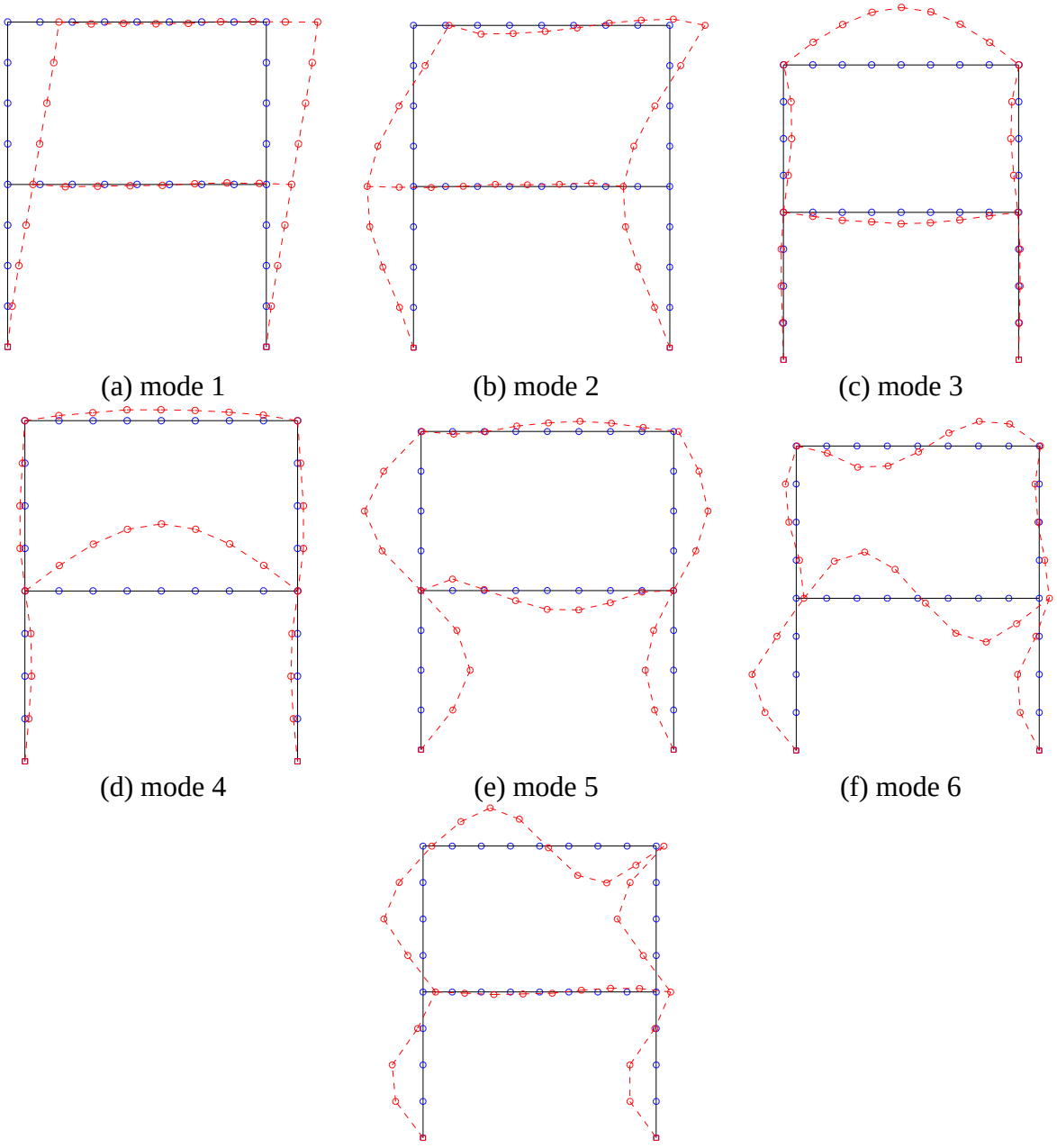

(a) mode 1 (b) mode 2 (c) mode 3

(d) mode 4 (e) mode 5 (f) mode 6

(g) mode 7

Figure 12. Measured mode shapes for undamaged steel frame.

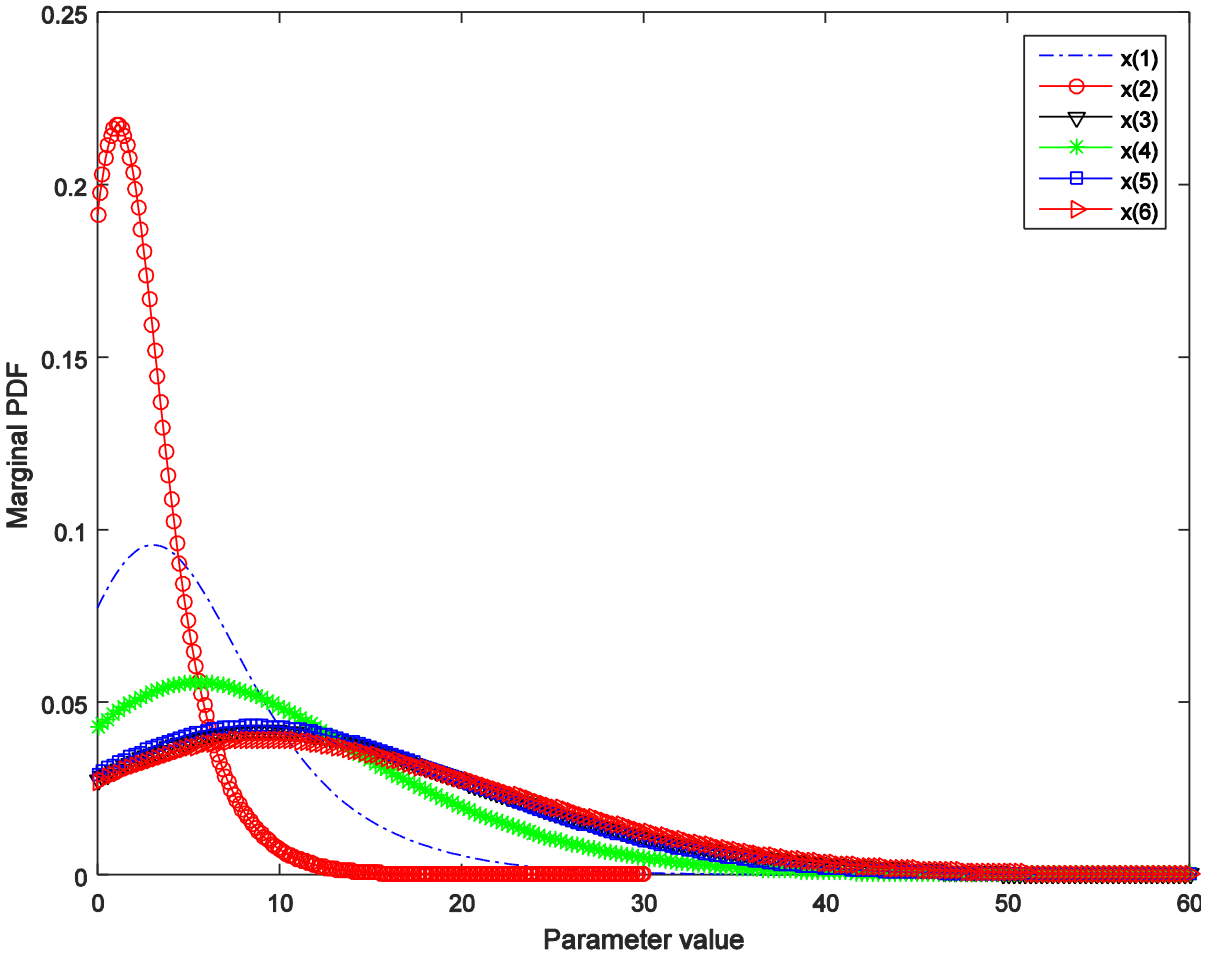

Figure 13. Posterior marginal PDFs of undamaged steel frame.

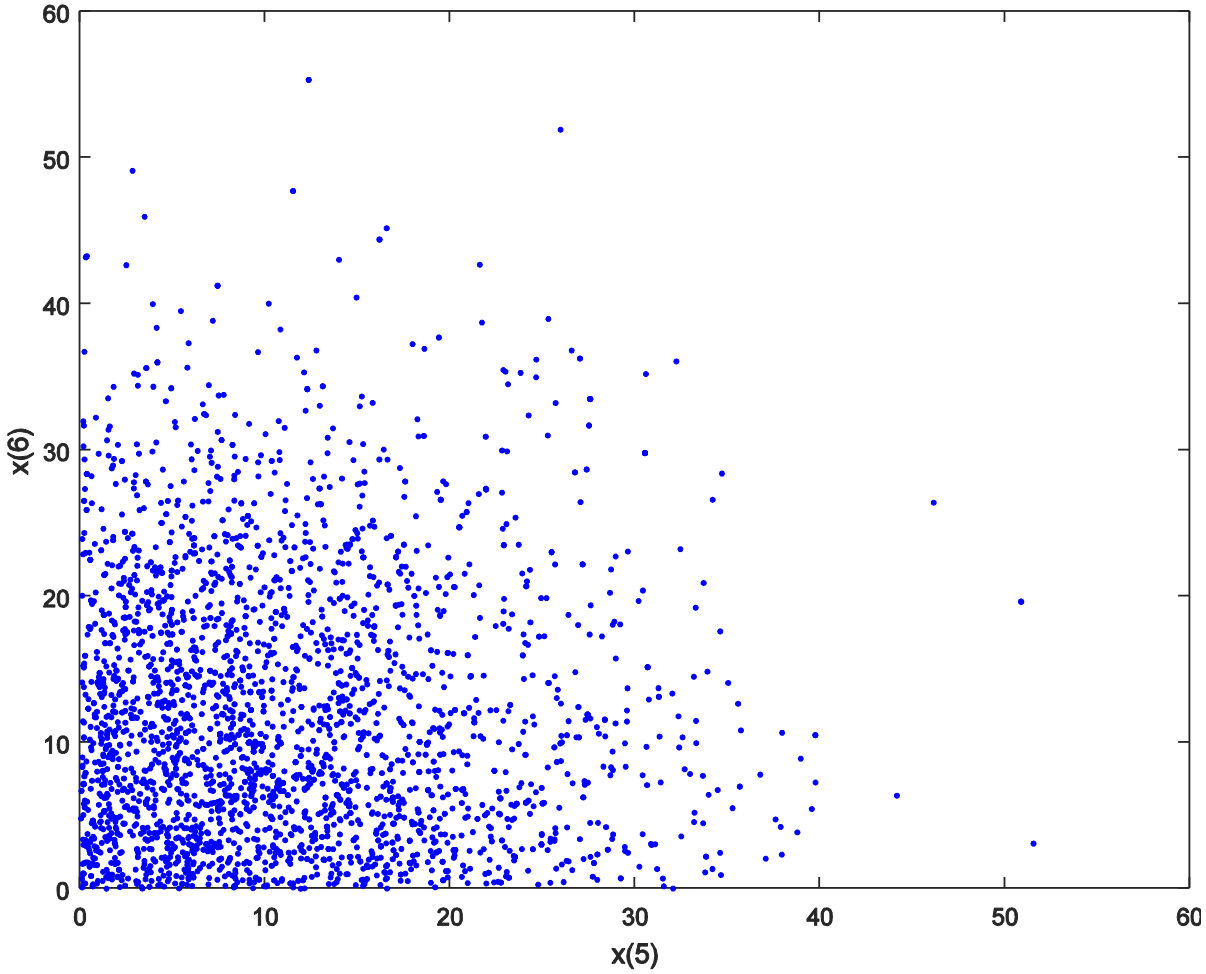

Figure 14. Projection of the posterior samples on the x(5)-x(6) plane.

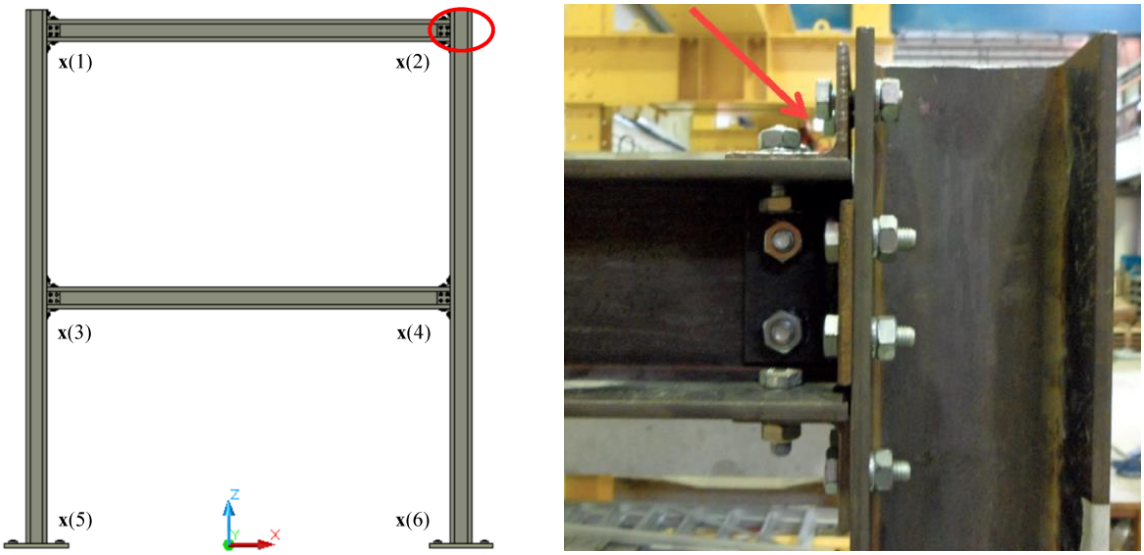

(a) Location of damage. (b) Details of damaged joint.

Figure 15. Damage case of steel frame.

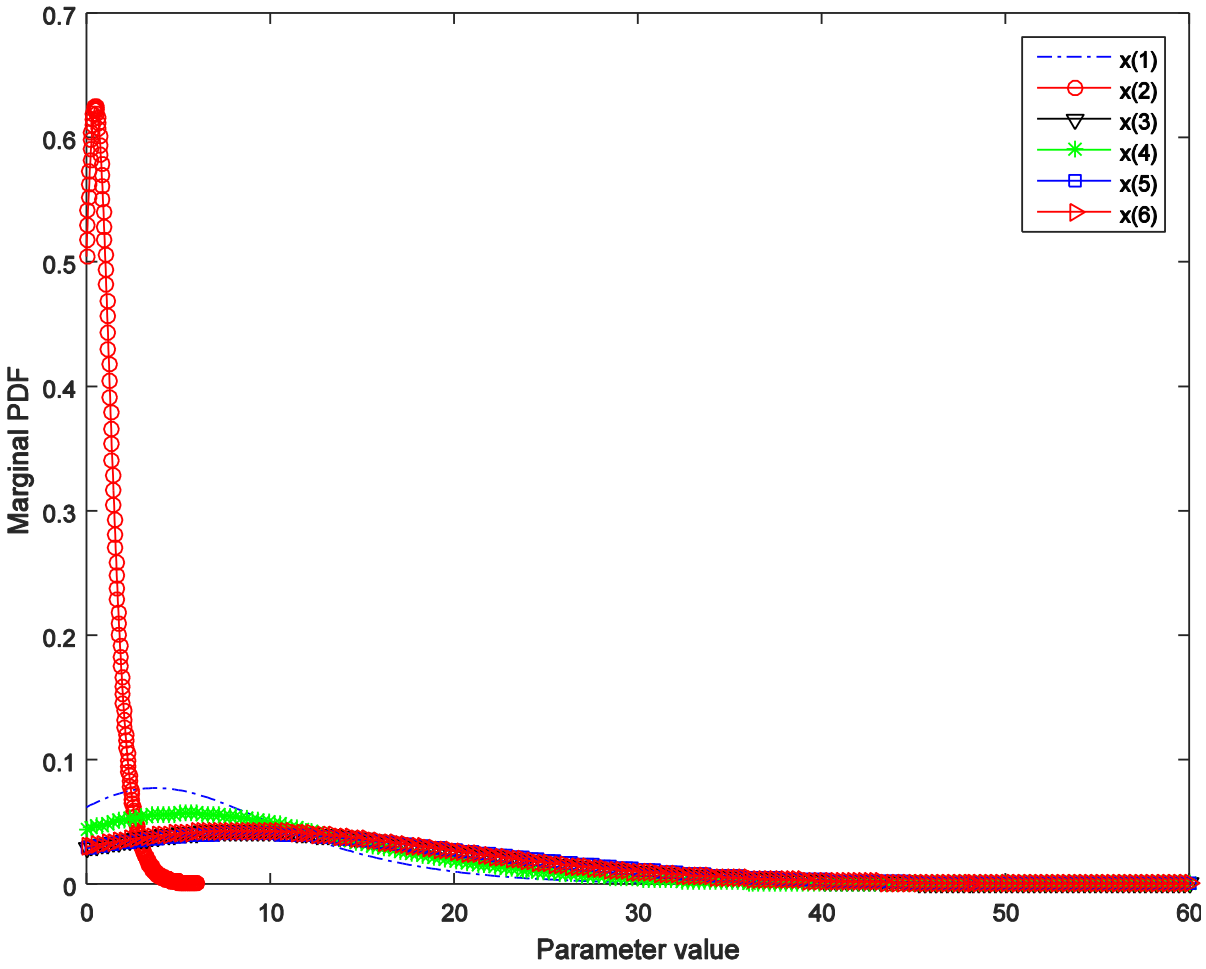

Figure 16. Posterior marginal PDFs of steel frame in damage case.

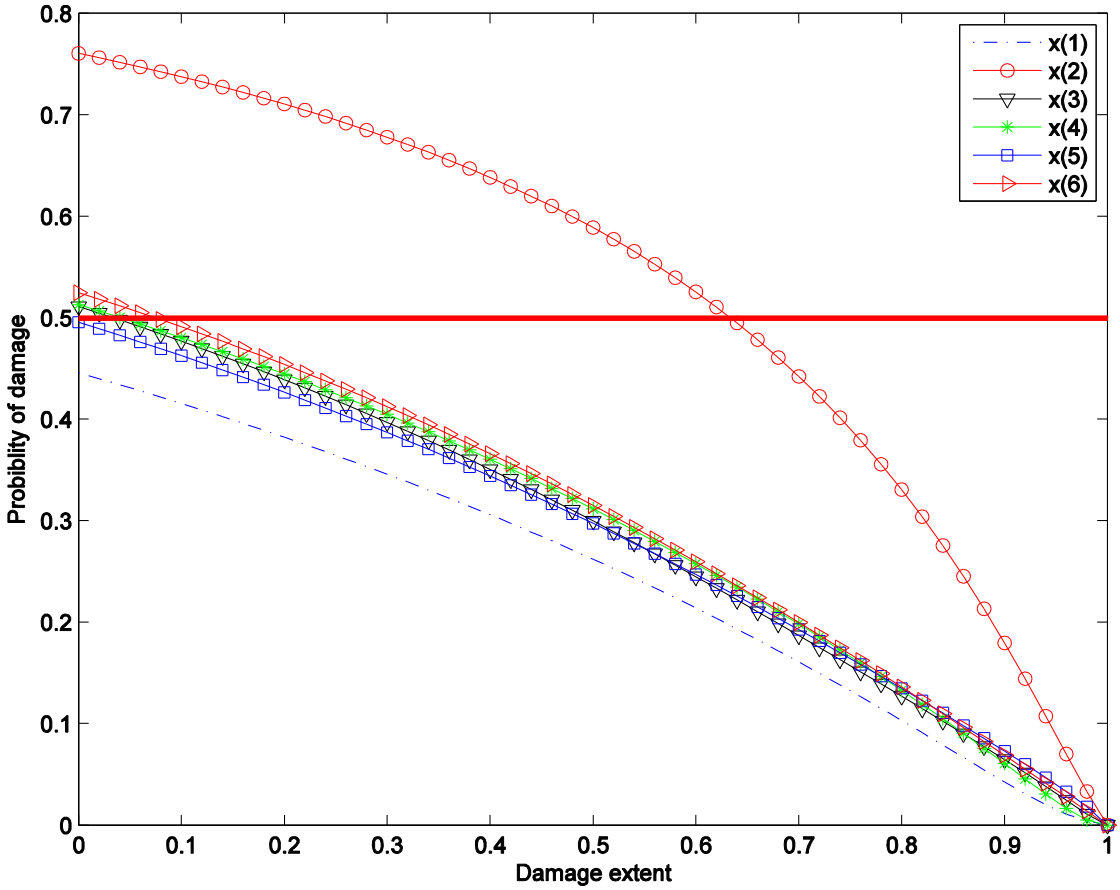

Figure 17. CDF of damage extent of steel frame.

Table 1. Dimensions and material properties of shear building.

	Story 1	Story 2	Story 3	Story 4
Story height (m)	0.278	0.546	0.546	0.530
Width of column (m)	0.025			
Thickness of column (m)	0.005			
Length of story plate (m)	0.45			
Width of story plate (m)	0.28			
Thickness of story plate (m)	0.025			
Young's modulus of steel (GPa)	200			
Mass of story plate (kg)	26.64	27.17	27.14	26.07
Inter-story stiffness (10^5 N/m)	1.1636	0.1536	0.1536	0.1679

Table 2. Identified natural frequencies of shear building.

Unit: Hz	Mode 1	Mode 2	Mode 3	Mode 4
	1.39	4.08	6.03	10.07

Table 3. Sample means and COVs calculated with MCMC samples.

		$\mathbf{x}(1)$	$\mathbf{x}(2)$	$\mathbf{x}(3)$	$\mathbf{x}(4)$
Four-mode case	Sample mean	0.8139	0.6854	0.7581	0.7690
	Sample COV	2.30%	3.48%	2.98%	2.03%
Two-mode case	Sample mean	1.0447	0.6836	0.7342	0.7520
	Sample COV	44.00%	4.79%	5.43%	3.12%
One-mode case	Sample mean	4.0834	0.6371	0.6764	1.2248
	Sample COV	77.43%	4.33%	7.53%	67.46%

Table 4. Identified natural frequencies for undamaged steel frame.

Unit: Hz	Mode 1	Mode 2	Mode 3	Mode 4	Mode 5	Mode 6	Mode 7
	16.78	69.85	109.14	114.87	253.82	373.19	412.89

Table 5. Nominal values of rotational stiffness.

Unit: Nm/rad	Location 1	Location 2	Location 3	Location 4	Location 5	Location 6
	5×10^{6}	5×10^{6}	1×10^{8}	1×10^{7}	1×10^{7}	1×10^{7}